Microfluidic Platform for *In Vitro* Study

on the Development of Cell Therapy

BY

YUAN XING
B.S., Wuhan University, Wuhan, Hubei, P. R. China, 2010
M.S., Illinois Institute of Technology, Chicago, IL, USA, 2012

THESIS

Submitted as partial fulfillment of the requirements
for the degree of Doctor of Philosophy in Bioengineering
in the Graduate College of the
University of Illinois at Chicago, 2017

Chicago, Illinois

Defense Committee:

Dr. Ying Liu, Chair, Chemical Engineering
Dr. José Oberholzer, Advisor
Dr. Yong Wang
Dr. Tolou Shokuhfar
Dr. Solomon Afelik, Surgery

ACKNOWLEDGMENTS

First of all, I am extremely grateful to my advisor, Dr. José Oberholzer, for the continuous support of my Ph.D. study and related research, for his patience, motivation, and immense knowledge. I am also thankful for the excellent example he has provided as both successful professor and surgeon.

Besides my advisor, I would like to thank the rest of my thesis committee: committee chair Dr. Ying Liu, Dr. Tolou Shokuhfar, Dr. Yong Wang and Dr. Solomon Afelik, for their insightful comments and encouragement, but also for the hard question which incented me to widen my research from various perspectives.

A special heartfelt thanks to my mentor, Dr. Yong Wang, for taking me under his wing. His guidance and all the useful discussions and brainstorming sessions, especially during the difficult conceptual development stage for every project. His “old man” deep insights helped me at various stages of my research.

I would also like to thank the team of Chicago Diabetes Project, fellow graduate students, research technicians, collaborators, and the multitude of undergraduates who contributed to this research. I am very grateful for all of you being there and supporting me for my research.

Words cannot express the feelings I have for my parents for their constant unconditional support – both emotionally and financially. I would not be here if it is not for you.

Finally, I would like to acknowledge the most important person in my life – my wife Yechen. She has been a constant source of strength and inspiration. There were times

during the past four years when everything seemed hopeless and I did not have any hope. I can honestly say that it was only her faithful determination and constant encouragement (and sometimes a kick on my backside when I needed one) that ultimately made it possible for me to see this road through to the end.

Yuan Xing

Chicago, IL

STATEMENT OF CONTRIBUTION OF AUTHORS

The chapter 2 of the following thesis contains methods and results from a previously published manuscript [Xing, Y., et al., A pumpless microfluidic device driven by surface tension for pancreatic islet analysis. *Biomedical Microdevices,* 2016. 18(5)], which I was the first author and, under the supervision of my advisor Dr. José Oberholzer and mentor Dr. Yong Wang, independently completed the device design and most of the testing with biomaterials provided by my colleagues in the lab. I organized figures and wrote the main body of manuscript, which had been reviewed and further improved by other corresponding authors before publication.

TABLE OF CONTENTS

TABLE OF CONTENTS (Continued)

TABLE OF CONTENTS (Continued)

LIST OF TABLES

LIST OF FIGURES

LIST OF FIGURES (Continued)

LIST OF FIGURES (Continued)

LIST OF ABBREVIATIONS

5-ALA	5-Amino-Levulinic Acid
ADP	Adenosine Diphosphate
AMP	Adenosine Monophosphate
ATP	Adenosine Triphosphate
BSA	Bovine Serum Albumin
CCD	Charged Couple Device
CDC	Centers for Disease Control and Prevention
CFD	Computational Fluid Dynamics
DI	De-Ionized
ECM	Extracellular Matrix
ELISA	Enzyme-linked Immunosorbent Assay
FBS	Fetal Bovine Serum
FDA/PI	Fluorescein Diacetate / Propidium Iodide
GCM2	Glial Cell Missing 2
GLUT-2	Glucose Transporter-2
GSIS	Glucose-Stimulated Insulin Secretion
hESC	Human Embryonic Stem Cell
hPSC	Human Pluripotent Stem Cell
HSC	Hematopoietic Stem Cell
iPSC	Induced Pluripotent Stem Cell
KRB	Krebs-Ringer Buffer
PBS	Phosphate Buffered Saline
PDMS	Polydimethylsiloxane

LIST OF ABBREVIATIONS (Continued)

PP	Pancreatic Polypeptide
PTH	Parathyroid Hormone
TIDM	Type I Diabetes Mellitus
TIIDM	Type II Diabetes Mellitus
TCA	Tricarboxylic Acid
UV	Ultraviolet
VDCC	Voltage-Dependent Calcium Channel
μ-PIV	Micro Particle Image Velocimetry

SUMMARY

Cell therapy has emerged as a treatment of many endocrine disorders. Microfluidics has been developed for a myriad of biological applications and the intrinsic capability of controlling and interrogating the cellular microenvironment with unrivalled precision. Development of microfluidic technologies has potentials to address cell-relevant biological phenomena, and aligns capabilities with translational challenges and goals.

Human islet transplantation is a promising cell-based therapy for Type I diabetes mellitus (TIDM). We developed a pumpless liquid delivery system driven by surface tension to significantly simplify the microfluidic operation for islet *in vitro* study. With the new device, an improvement can be achieved with lower material consumption, increased assay sensitivity, accuracy, and higher spatiotemporal resolution.

Hypoparathyroidism is an uncommon condition associated with abnormally low levels of parathyroid hormone (PTH), leading to low calcium levels in blood and bones and to an increase of serum phosphorus. Allotransplantation of encapsulated parathyroid cells is an alternative treatment without immunosuppressants, while avoiding complications of supplemental therapy. We are able to manipulate the flow in microfluidic channels of our new microencapsulator device and efficiently generate the micro-encapsulated cells (with the size of <100 μm), which can be the answer to the future cell therapy of hypoparathyroidism.

Furthermore, cell therapy treatment strategies also include isolation and transfer of specific stem cell populations, administration of effector cells, induction of mature cells

to become pluripotent cells, and reprogramming of mature cells. To acquire the sufficient information of cell reprogramming, understand the cell physiological mechanisms, and test the function of potential cellular products, we designed a new perfusion chamber device allowing us to perform the efficient perfusion at the single cell level.

1. INTRODUCTION

1.1 Cell Therapy

The origins of cell therapy, which is injecting cellular material into a patient, can be traced back to the nineteenth century when Charles-Édouard Brown-Séquard injected animal testicle extracts to try to alter aging effects.[1] In 1931, Paul Niehans, known as the pioneer of cell therapy, attempted to cure a patient by injecting material from calf embryos.[2] In 1953, researchers found that recipient animals could be made to not reject transplanted organs by pre-inoculating them with cells from donor animals. In 1968, the first human bone marrow transplantation was successfully performed in Minnesota.[3]

Over past decades, cell therapy has emerged as a strategy for the treatment of many human diseases. As reported previously from Finance and Investment Club in Boston University, shown in Figure 1, the market of cell therapy product has been expanding dramatically and will keep growing.

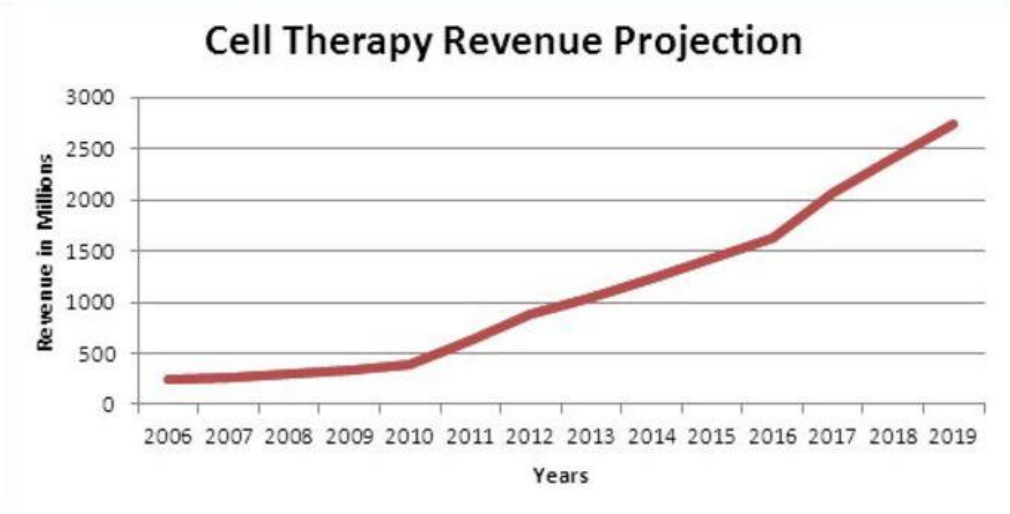

Figure 1. Trends of cell therapy market expansion. Adopted from a presentation by Matthew Sgrignari in Boston University, Finance & Investment Club.

There are mainly two categories of cell-based therapies: allogenic cell transplantations and stem cell based therapies. In allogenic cell therapy, primary cells, tissues, or organs are transplanted into a recipient from a genetically non-identical donor. In 1967, Christiaan N. Barnard, a South African surgeon, performed a human heart transplantation. Transplants of hearts, kidneys, and other vital organs are now being performed at an increasing rate throughout the world. Stem cell therapies, on the other hand, use stem cells or stem cell-derived cell types to treat or prevent a disease.[4] In the past 30 years, bone marrow was the only widely used stem cell therapy to treat cancer patients with conditions such as leukemia and lymphoma.[5] However, researchers are developing various sources to apply stem-cell treatments for neurodegenerative diseases, endocrine disorder conditions and cancer. Stem cell therapy holds the promise to treat many disease, and repair damaged tissues in patient bodies, since there are currently no or limited therapeutic options, such as diabetes. Over decades, the potential of stem cell therapies has been recognized and improved, specifically, the development of induced pluripotent stem cells (iPSC) has further enriched the stem cell field. However, the stem cell based clinical products also remains unanticipated risks. There are many risk factors of stem cell based products leading to failure of stem cell applications, including the stem cell type, their differentiation and proliferation capacity, *in vitro* culture and the route of administration, the target location, irreversibility of treatment, and long-term survival of engrafted cells. All these factors, together, determine the risk profile of a stem cell based clinical product. In previous experiences of animal experiments and human clinical trials, identified risks included tumor formation, unwanted immune responses, and the

transmission of adventitious agents, which showed high chance to lead lethal conditions.[6]

1.2 Microfluidic Techniques

As an important part of development of microfabricated bioanalytical systems, “microfluidics” may be defined as the precise manipulation of fluid flow at a length scale of several to hundreds of microns. In microfluidic devices, high-fidelity patterning of micro-structures, such as channels, chambers, valves, and membranes, are commonly made of elastic silicone polymer (PDMS), thermoplastic materials (e.g., polystyrene and polycarbonate), and glass. At micro-sized scales, fluid flow are simplified and highly predictable, allowing engineers to manage multiple environmental conditions, including temperature, pH, dissolved gas concentration, shear stress, and medium exchange rates.[7] To achieve different goals of applications, microfluidic chips are then designed with various microfluidic channel geometries, integrated with various microfluidic components and optical/electrical systems, such as micro-pillars, valves and electrons.

Microfluidic technique is attractive mainly due to their micro-scale dimensions and associated low inertia. The small size means low volume of fluid and consequently low material consumption in these systems. When samples have very limited resources, it is clear that microfluidic device shows its huge advantage. Also, due to the small overall size for a design of single working unit, it is easy to achieve massively parallel fluidic operations in different conditions or treatments, which would save enormous amounts of operation time. Benefit from tiny size design, high spatial resolution analysis is enabled in microfluidic devices. As summarized in Figure 2, operations conducted in microfluidic platforms offer the possibility of portable sample substances, multitasking with parallel

fluidic designs. Low inertia, as another consequence of small size of microfluidic devices, can also benefit many research applications, especially for sensing of multiple elements and molecules, due to its advantages in high temporal resolution, fast response, low energy consumption and high sensitivity. Due to these advantages, microfluidic devices can be applied at the cell cluster, single-cell, or even subcellular levels in biomedical research.[8]

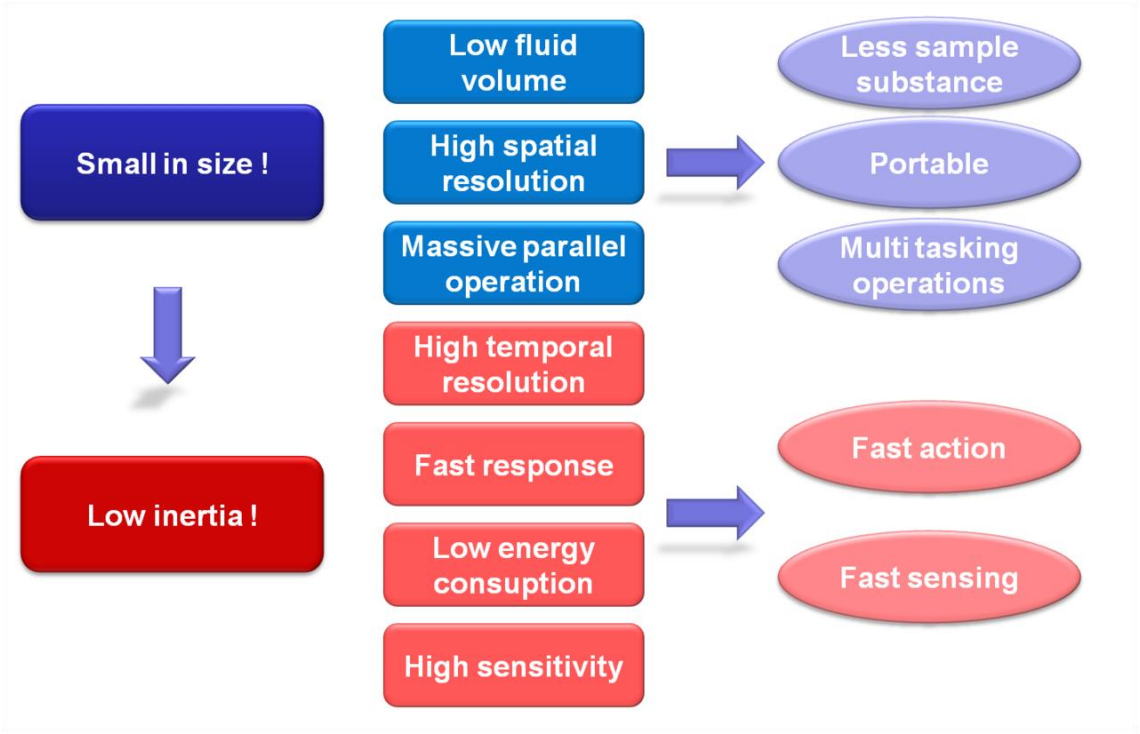

Figure 2. Advantages of microfluidic techniques. Adopted from https://en.wikiversity.org/wiki/Microfluid_Mechanics/Introduction.

Photo- and soft-lithography are widely used for the fabrication of microchannels.[9] In general, photo-lithography is used to allow micropatterning on a silicon wafer, which becomes a mold for soft-lithography, as shown in Figure 3A. To fabricate masters using photo-lithography, firstly, a spin-coated photoresist layer is selectively exposed to the UV light through a photomask, and a developing reagent is used to dissolve the non-crosslinked photoresist regions. Types of photomask and photoresist used in this procedure determine the fabrication resolution. Fabrication process for the master is commonly done in a clean room or inside a perfume hood in case the dust flying in the air affect the fabrication of small features. Despite the complex of master mold fabrication, an elastomer such as PDMS can be poured on the mold and subsequently cured to form the PDMS channel to easily replicate its surface structures and features. PDMS replica layers can be repeatedly fabricated and gently peeled off from a single silicon master without damage to the photoresist patterns. Figure 3B shows final steps of finishing a device. A piece of PDMS can be bonded to another piece of PDMS or glass substrates to form the micro features with O_2 plasma treatment, proper heat and pressure.[10] Because O_2 plasma creates hydroxyl groups that will form covalent bonds when they come in contact with hydroxyl groups on another surface. Bond strength can be further enhanced by pressure and thermal curing.[11]

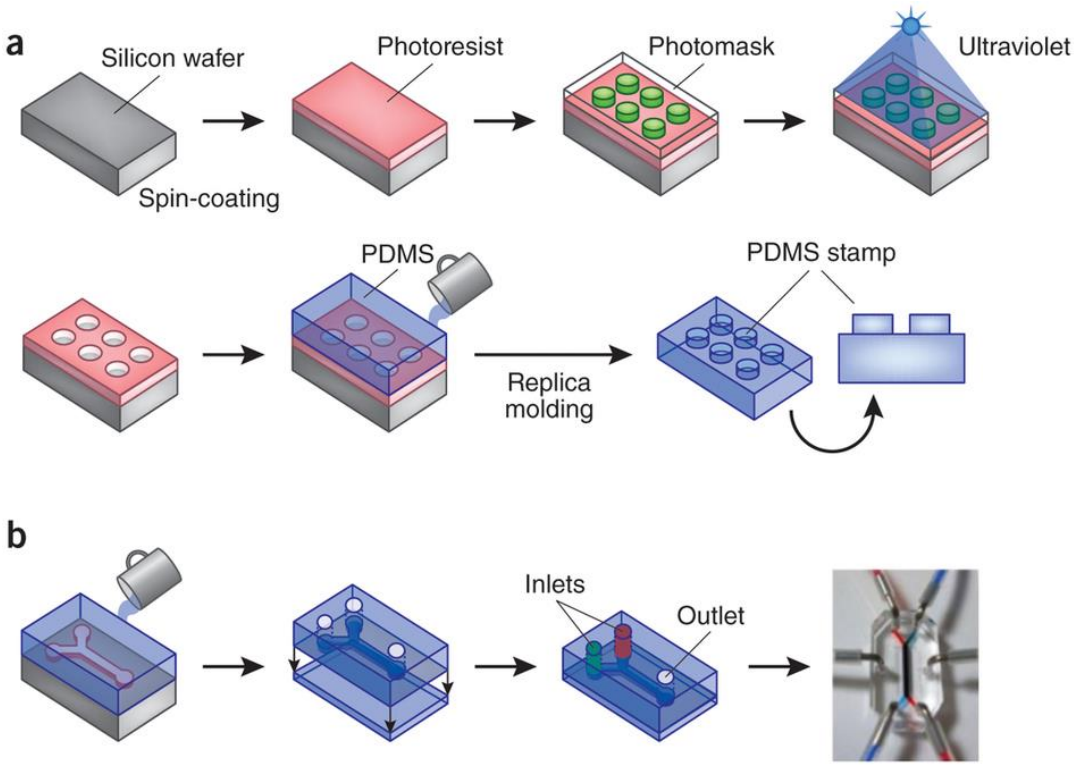

Figure 3. Fabrication of PDMS-based microfluidic devices. A: Photo- and soft-lithography steps of fabricating a single layer of PDMS. B: Finishing steps of device fabrication. Adopted from reference [10].

1.3 Microfluidic Applications for Cell-based Therapy Development

Regardless of types of stem cell, substantial barriers to clinical translation still exist and must be overcome in order to realize full clinical potential. Some are mainly technical issues, like cell isolation, derivation, expansion and differentiation, other challenges include quality control, bioprocess production monitoring, cost control. As Titmarsh D. M. et al summarized previously, the development of a typical cell-derived therapy will include the following steps: (shown in Figure 4)[12]

- Cell isolation, derivation, and/or enrichment
- *Ex vivo* cell expansion, differentiation, and harvesting
- Cell analysis and characterization of viability, potency, and batch quality
- Packaging, preservation, and administration
- Post-implantation monitoring

Uncertainties exist and must not be ignored in each of these cell-processing operation steps, thus, new technologies are necessary from both basic research and bioprocess development to improve the quality of cellular products in cell based therapy. As described above, microfluidics has been developed for many biological applications because of its intrinsic capability to precisely control and interrogate the cellular microenvironment, which is particularly relevant to optimizing bioprocesses within these steps. Development of microfluidic technologies has potentials to address cell-relevant biological phenomena and align capabilities with translational challenges and goals in the development of cell-based therapy.

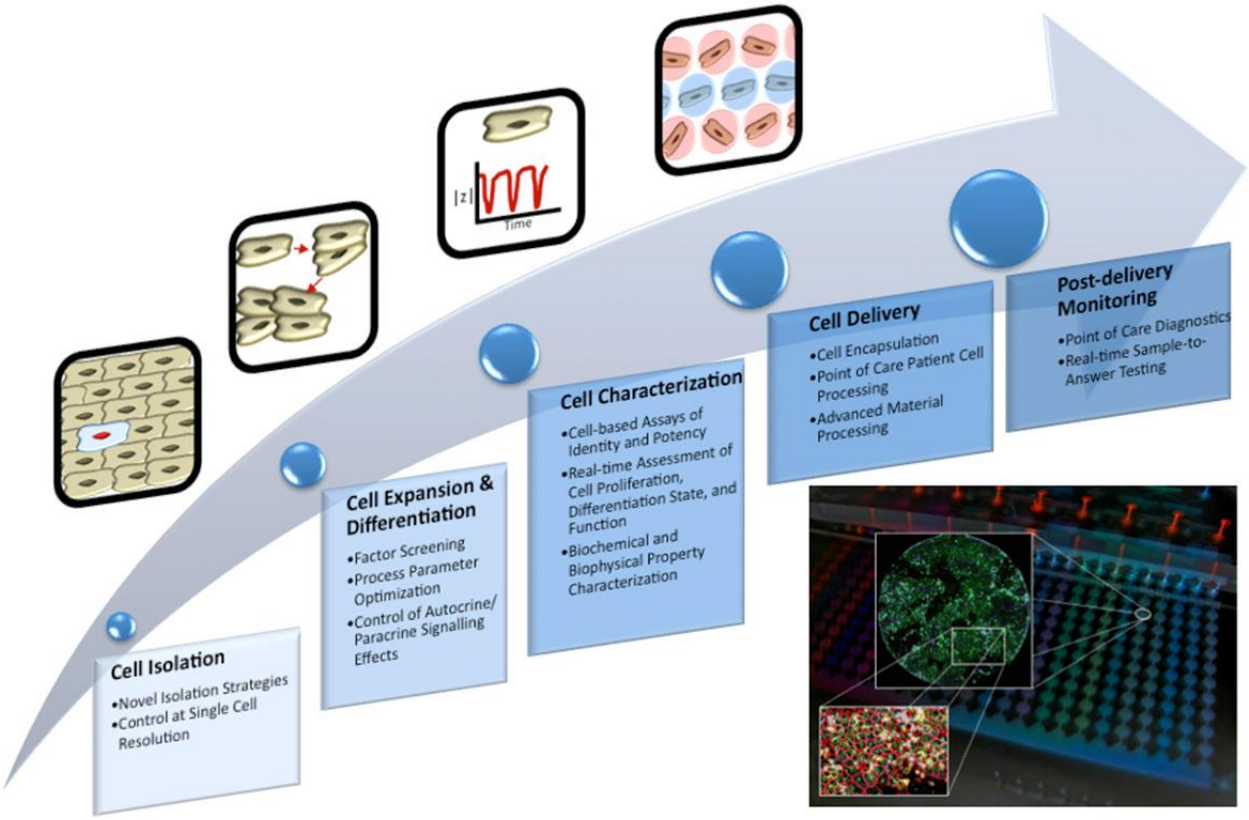

Figure 4. Microfluidic applications in cell-based therapy development. Adopted from reference [12].

2. A PUMPLESS MICROFLUIDIC DEVICE FOR *IN VITRO* STUDY OF ISLETS

I have used some major parts of my published works [13] with the permission from the publication which is included in Appendix.

2.1 Introduction

2.1.1 Pancreas and Islets of Langerhans

The pancreas is a glandular organ with both exocrine and endocrine functions. It has four different components: the exocrine tissue (98%), the endocrine cells (1-2%), the ducts, and the connective tissue.[14] Exocrine cells are responsible for releasing digestive enzymes for nutrient digestion, and endocrine cells, on the other hand, play key roles in the metabolism of glucose by secreting several hormones (Figure 5). The endocrine regions within the pancreas, known as the islets of Langerhans, contain five different cell types.[14, 15] 15-20% of the islet cells are alpha cells that are responsible for glucagon secretion that can cause the liver to convert stored glycogen into glucose during periods of hypoglycemia. 65-80% of the islet cells are beta cells, and they produce and secrete insulin, which is essential for the breakdown of glucose. Insulin secretion is primarily controlled by the glucose-stimulated and secretion pathway.[16] Delta cells, which make up 3-10% of islet cells, produce somatostatin that can suppress the secretion of other hormones made in the pancreas.[17] Pancreatic polypeptide (PP) cells, or gamma cells (3-5% of total islet cells), release pancreatic polypeptides to regulate both the endocrine and exocrine pancreatic secretions.[18] The last cell type found in islets is called the epsilon cell, which compose ~1% of islet cells and produce the “hunger hormone”

ghrelin.[19] In average, approximately one million islets distribute throughout an adult human pancreas. Adult human islets range in size from 50 to 300 μm in diameter and there are about 1,000-2,000 individual cells in each islet.[14] In addition, the exocrine tissue separates from the endocrine cells by dense capillary networks and glial sheets.[20] The capillary structure help the delivery of oxygen and glucose to islet cells as well as hormone secretion from islets.

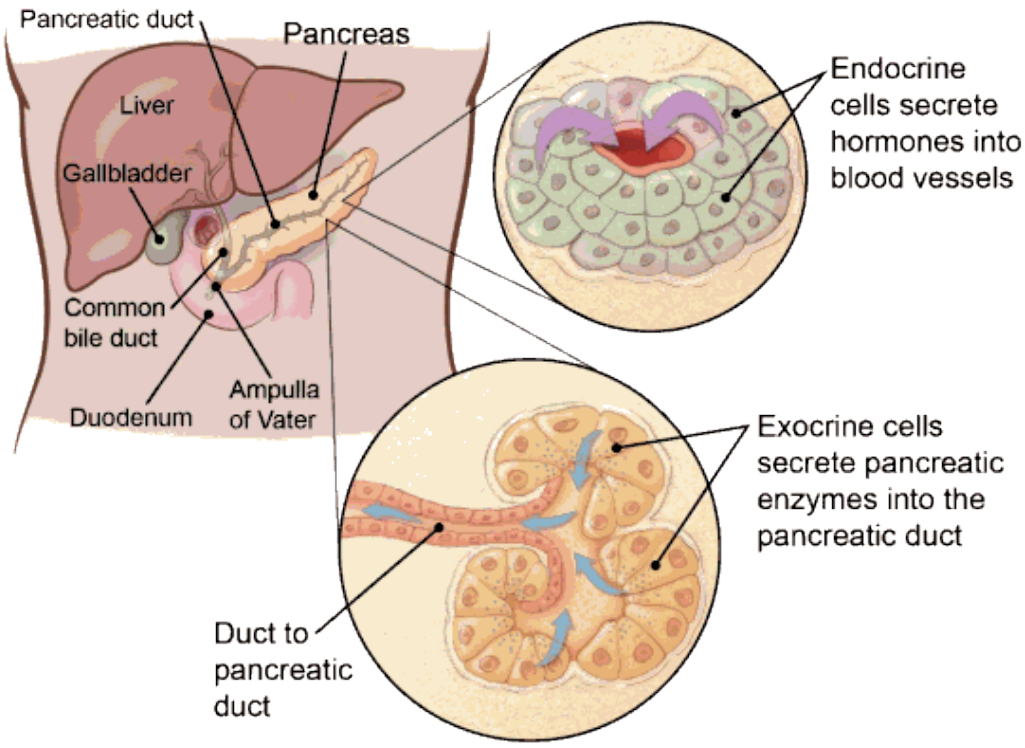

Figure 5. Human pancreas. Adopted from American Cancer Society.

2.1.2 Diabetes and Classification

Diabetes is a disease in which the blood sugar level is too high resulting from failure of insulin secretion and insulin function. The chronic hyperglycemia of diabetes is may cause vaginal and skin infections, slow healing cuts and sores, worse vision, stomach and intestinal problems and damage to eyes blood, vessels, nerve and kidney. Both the number of cases and the prevalence of diabetes have been steadily increasing over the past few decades.[21] Globally, an estimated 422 million adults were living with diabetes in 2014, compared to 108 million in 1980. The global prevalence (age-standardized) of diabetes has nearly doubled since 1980, rising from 4.7% to 8.5% in the adult population, as shown in World Health Organization (WHO) database. Based on data from the Central Disease Control (CDC), shown in Figure 6, the US had about 7.4% of the total population, which is near 23.5 million people, diagnosed with diabetes (Type I or II) in 2015.

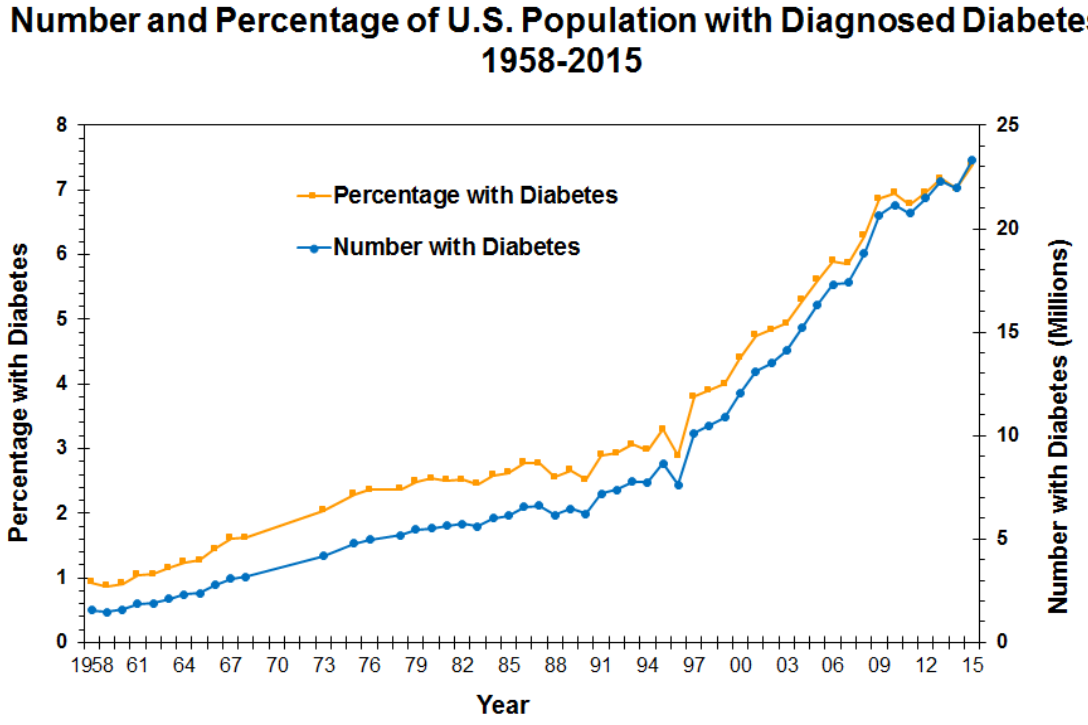

Figure 6. Number and percentage of U.S. population with diagnosed diabetes, 1958-2015. Adopted from Centers for Disease Control and Prevention (CDC).

As shown in Figure 7, there are two types of diabetes, referred to as Type I diabetes mellitus (TIDM) and Type II diabetes mellitus (TIIDM), which have completely different biomolecular mechanics of their insulin deficiency.[22]

Type I diabetes was once known as juvenile diabetes or insulin dependent diabetes, and it accounts for 5-10% of all diabetes patients. TIDM happens when immune systems destroy β-cells in the pancreatic islets leading to the inability to produce insulin. In the development of TIDM, the β-cell destruction rate shows huge difference in between individuals of TIDM patients. For instance, the islet cells damaged much faster in children than in adults. Ketoacidosis, a complication of TIDM with a metabolic state associated with high concentrations of ketone bodies, is often developed in new or untreated TIDM patients. Unlike the children, adults have many regulation pathways to affect β-cell function to prevent ketoacidosis. However, the TIDM patients who must prolong their life expectancy with insulin treatment show a higher risk to develop ketoacidosis. As this disorder developed to a much later stage, insulin secretion is very limited or undetected, as resulted from extremely low plasma C-peptide levels. TIDM can happen at any age, and caused by not only genetic reasons but also environmental factors, although many of reasons are still unknown. Patients identified with TIDM are less expected to be obese, but they are often diagnosed with other types of autoimmune disorders. Beside lifestyle management, like controlling diet and exercise, injections of insulin are necessary for TIDM patients. Due to the hypoglycemia and other side effects, researchers and physicians are looking for other treatments as insulin replacements to better solve the conditions patients are suffering from disease.[22]

Type II diabetes makes up about 90-95% of cases of diabetes. In comparison to TIDM, Type II diabetes has been previously known as adult or non-insulin dependent diabetes. TIIDM patients usually have insulin resistance and relative insulin deficiency which cause high blood sugar level. Though the specific causes are not known, TIIDM primarily occurs as a result of obesity and unhealthy lifestyle, due to their capability to cause insulin resistance. Type II diabetes is difficult to diagnose and thus often lurking for years as hyperglycemia progresses, since it is very hard to find some typical symptoms of diabetes in early developed TIIDM. Unlike TIDM, ketoacidosis is not observable in Type II diabetes patients. For TIIDM, insulin injections are not very useful due to the resistance of insulin function. Disease condition may be alleviated in patients who actively improve their live habits with the help of medication. However, for these patients, it is nearly impossible to return to normal insulin secretion level.[22]

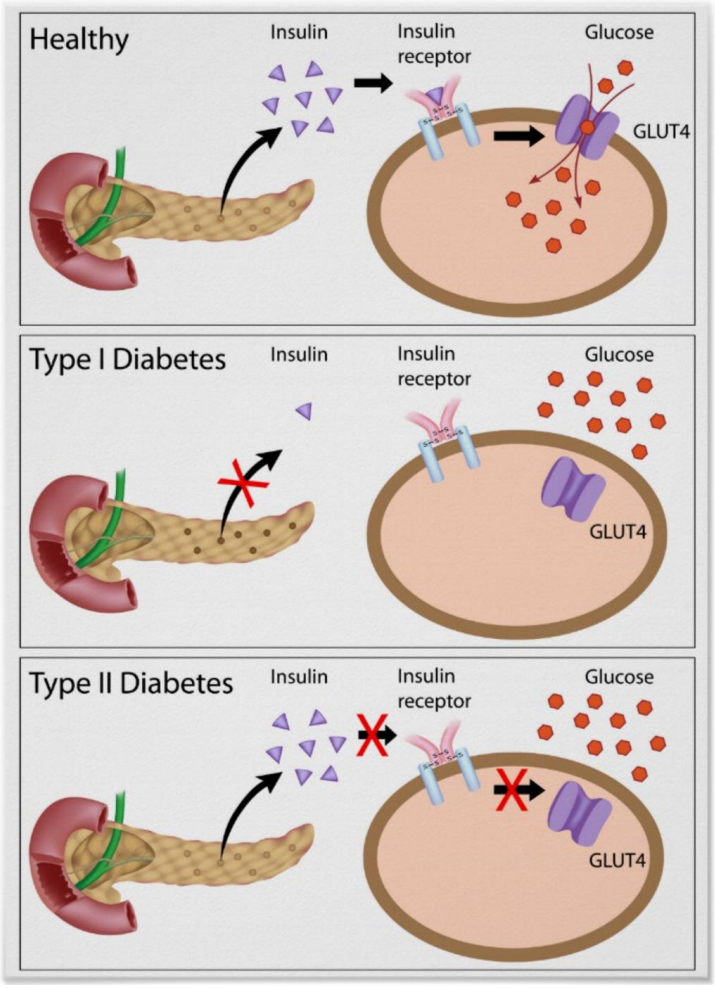

Figure 7. Type I and Type II diabetes. Adopted from Alila Medical Media, Co.

2.1.3 Clinical Islet Transplantation

Currently, the clinical islet transplantation, as a cell based therapy aiming to permanently cure patients relying on daily insulin injection and treatment, holds most promises among all insulin independent therapies for TIDM patients (Figure 8). A pancreatic islet transplant surgery is easy, fast and non-invasive. The surgery itself usually takes less than an hour to complete, and the patient can go home within 24 hours of the procedure.

The idea and first attempt of pancreas transplantation can be traced back to 1894, Williams used sheep pancreas pieces and extracts for oral and subcutaneous therapy to treat diabetes and reported failure.[23, 24] In 1972, Ballinger and Lacy found that the blood glucose level can be brought back to normal after implant islet isografts in diabetic rats.[25] After a lot of effort by investigators, finally, in 1980s, the first successful case of islet auto-transplantation was reported.[26, 27] For the preparation of islet autografts, a total pancreatectomy is performed in patients with severe and chronic pancreatitis. Followed, the pancreas undergoes enzymatic digestion at controlled temperature and time, and further purified for transplant that isolated islets are injected into the portal vein of patient. By 1995, 70% of islet auto-transplantation treatment were reported as successful cases in those patients receiving more than 300,000 individual islets.[28]

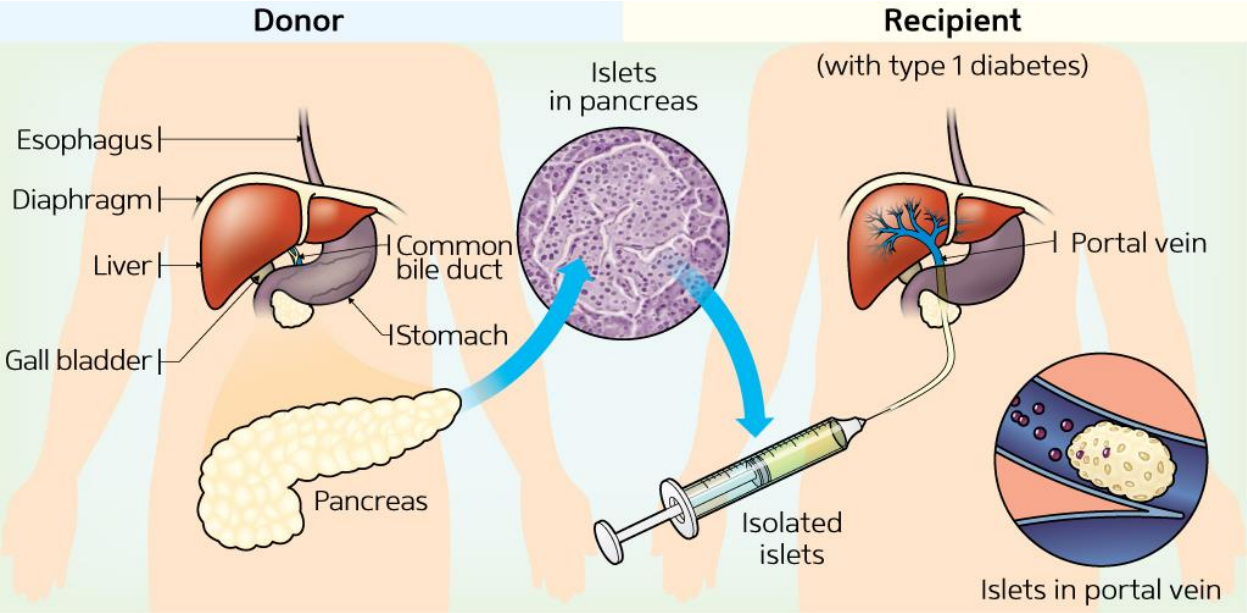

Figure 8. The process of clinical islets transplantation. Adopted from reference [29].

While autograft method is not usable for TIDM patients due to the autoimmune attack, the first human islet allotransplantation was also successfully conducted in 1980s. By 2005, 65 TIDM patients in total accepted islet allotransplant, but only 10% of them became insulin independence and 80% of patients were C-peptide positive and kept receiving insulin injection, other 10% were failed.[30, 31, 32] Islet cells transplantation is promising to treat TIDM, but still remains limitations to this treatment. A key factor is that enough high quality purified islets must be yielded from each isolation and ready to transplant.

Steps of general procedure of islet isolation are illustrated in Figure 9. Firstly, after collagenase is infused into the pancreas, organ is chopped into pieces and being maintained at proper temperature for digestion using Ricordi chamber. Then, islets freed from surrounding tissue are purified from exocrine tissue using a density based separation method. Maintenance of isolated islets is another main limitation of yield of islet isolation, since number of islets are lost dramatically during cell culture. The cause of islet cell loss is considered to be the insufficient supply of nutrition. Because, in pancreas, complicated vasculature networks, which would be disrupted during islet isolation process, ensure the delivery of nutrients through blood stream to cells. Another factor that affects the survival and function of implanted islets is hypoxia, which is resulted from the low oxygen condition in liver.[23, 33]

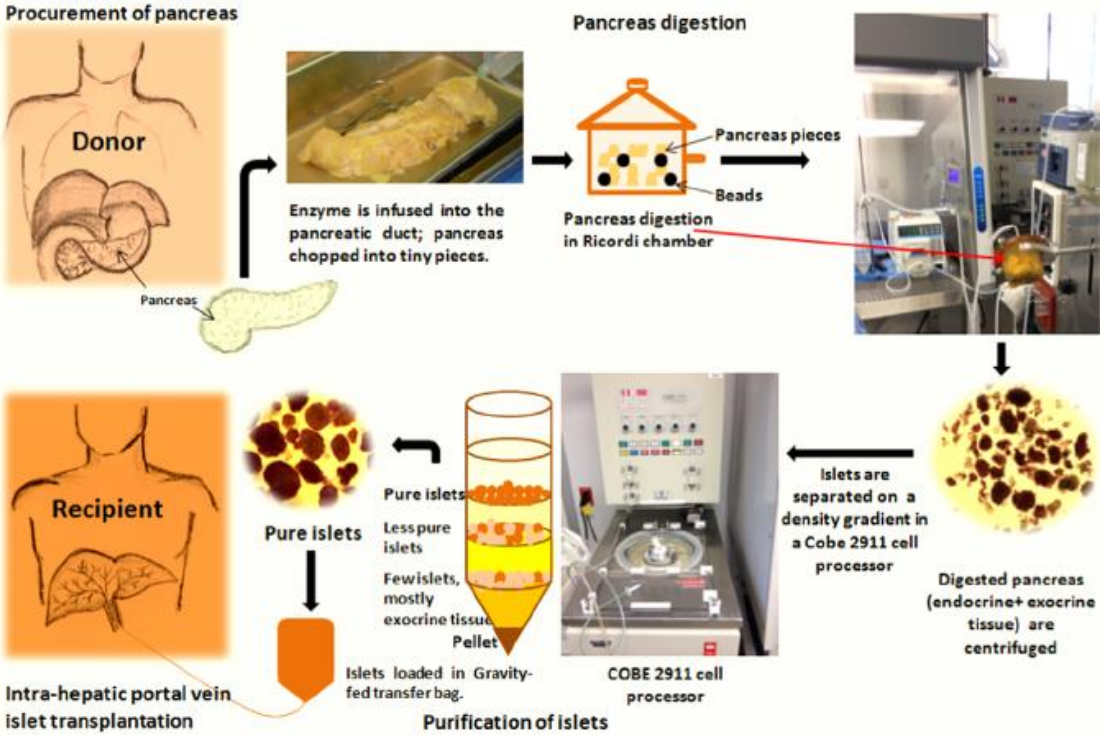

Figure 9. The procedure of clinical human islet isolation. Adopted from reference [33].

The major problem to be overcome in transplantation therapy is rejection, an immune phenomenon. After transplantation, the body recognizes the transplanted tissue cells as antigens and immediately sets up an immune response by producing antibodies. These antibodies are capable of inhibiting metabolism of the cells within the transplanted organ and eventually actively cause their destruction. In addition, the blood-mediated inflammatory reaction promotes platelets formation, which subsequently induce forming fibrin. The fibrin influences macrophages that promotes inflammatory reactions, which is another main contributor to islet loss.[23] The immunosuppressive drugs are often used to inhibit immune response from recipient immune system and stop the destruction of the implanted islets.

2.1.4 Islet Perifusion and Evaluation

Pancreatic islet beta cells are capable to sense high blood sugar level and secret insulin in response. The primary nutrient secretagogues for insulin stimulus is glucose in blood. As shown in Figure 10, glucose-stimulated insulin secretion (GSIS) shows a biphasic and pulsatile kinetic profile in response to the dynamic changes of glucose concentration, and this process is precisely coupled with multiple intracellular signaling pathways and factors such as metabolic process, calcium ion influx and membrane potential change.[34-37] The blood glucose binds and transports through glucose transporters 2 (GLUT-2) in beta cell membrane and undergoes glycolysis to produce pyruvates, which further enter Tricarboxylic Acid Cycle (TCA cycle) in mitochondria and consequently go through oxidative phosphorylation to produce ATP. The ATP-sensitive K^+ channels (K_{ATP}) closed subsequently induce the cell membrane depolarization and an increase of intracellular calcium ions via voltage-dependent calcium channel (VDCC). The

$[Ca^{2+}]_i$, behaves as a second messenger, then triggers the release of insulin from insulin granules.[38, 39] Insulin secretion from beta-cells has a biphasic profile: a sharp peak within 3-5 min post-stimulation of high glucose and slowly increasing secretory rate with continuous high glucose stimulation. The pulsatility of insulin secretion, as another important feature of insulin secretion, has been shown in simultaneous measurement of $[Ca^{2+}]_i$ and insulin secretion. From previous observation, oscillation rate varies from 1 minute/cycle to 7 minute/cycle and highly depends on resource species and cell function.[40] There is evidence showing that other glucose-related metabolic signals can also affect oscillations of insulin secretion, although effects are much less than that of calcium ion oscillations.[41] More interesting studies showed that there are some unknown mechanics beside K_{ATP} channel-dependent pathway for insulin secretion. Researchers tested mice with genetic disruptions of K_{ATP} channel subunits, and found that they were still able to secrete insulin in response to high glucose stimulation.[42]

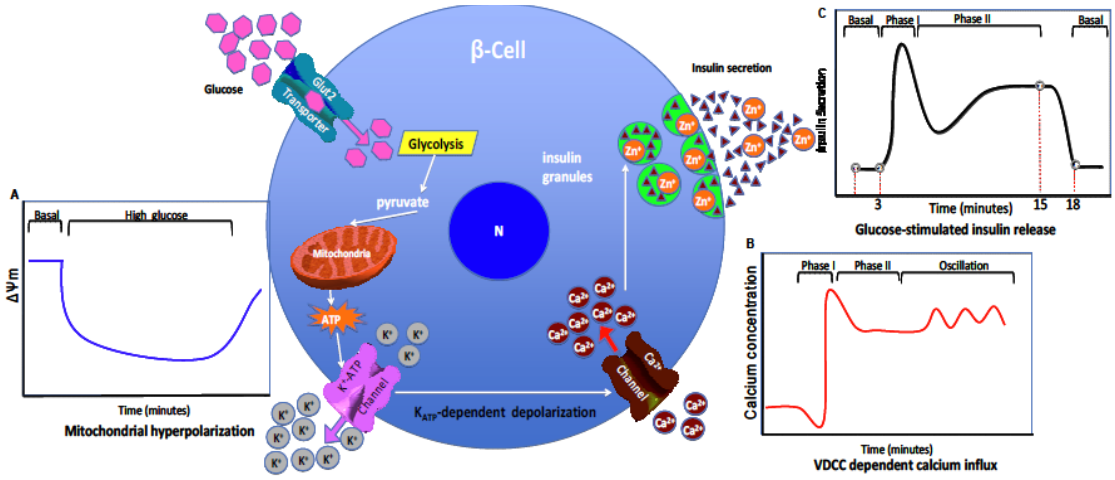

Figure 10. Glucose-stimulated signaling pathways and kinetics of insulin secretion. A: Glucose-stimulated mitochondrial hyperpolarization. B: VDCC-dependent biphasic $[Ca^{2+}]_i$ and oscillation. C: K_{ATP}-dependent biphasic insulin secretion.

Perifusion systems to challenge islets with glucose and measure dynamic insulin release have been utilized for more than 35 years and remain a valid procedure used by many research laboratories to evaluate islet function in a more physiologically relevant way.[43-46] Also, this method is useful for determining regulation of hormone release in response to various drugs and agents.[47-50] In brief, buffer solutions containing different glucose concentrations or other drugs are utilized to stimulate isolated islets continuously, and thus, insulin secreted from islet beta-cells are collected over time during the perifusion for later measurement.[51, 52] Meanwhile, cell signaling information, like mitochondrial activity and intracellular calcium level, can also be acquired dynamically by using specific fluorescent tracers.

2.1.5 Current Microfluidic Platforms for *In Vitro* Study of Islets

Many attempts have been done to build platforms for *in vitro* study of islets. Over decades, several macro-scale perifusion systems were reported that they are capable to control temperature, pH, and flow rate of the perfusate solutions in an islet perifusion assay. However, it is hard to precisely control the fluid flow, cell microenvironment in macro-scale systems. Moreover, needs of sample volume and material consumption are out of control due to the large size of design. Microfluidic devices, in this case, are particularly suitable to simplify perifusion apparatus with the additional advantage of the ability to simultaneously conduct other assays, such as fluorescent imaging. More important thing is, the micro-scale devices provide finer control of fluid delivered to islets allowing a better mimicked microenvironment of *in vivo* flow volume of the pancreatic vascular system.

In past decades, several well developed microfluidic systems for islet *in vitro* studies have been reported. The Kennedy group showed a Borofloat glass device for insulin measurement from stimulated islets.[53] The Piston group designed a single layer PDMS device to study cell-to-cell communication in between islet cells.[54] The Ismagilov group designed a chemistrode generating pressure driven droplets to deliver different chemicals for precise islet physiological studies.[52] The Roper group integrated a PDMS device with on-chip pump and mixer for islet perifusion assays.[55] Since 2009, we have also developed several perifusion-based microfluidic devices that are specialized for islet and beta-cell research.[56-58]

As described above in 1.2, these microfluidic devices have many advantages over the traditional macroscale perifusion apparatus; however, they also have some limitations that can hamper their adoptability and use in wider applications in the field of diabetes research and treatment. For example, like most of the microfluidic devices, these systems need macro-scale pumps and other accessory components to facilitate flow delivery and perifusate collection. Figure 11 shows the complexity of experimental setup of a typical microfluidic assay, which needs external energy sources, such as a pump, for the steady delivery of fluids. External pumps are often bulky and operationally burdensome, which is completely inconsistent with the simplistic philosophy of a microfluidic system. Additionally, accessory components, such as syringes and tubing, can increase liquid/analytic reagent consumption, lead to bubble generation, and reduce spatiotemporal resolution of measured hormones and physiological activities.

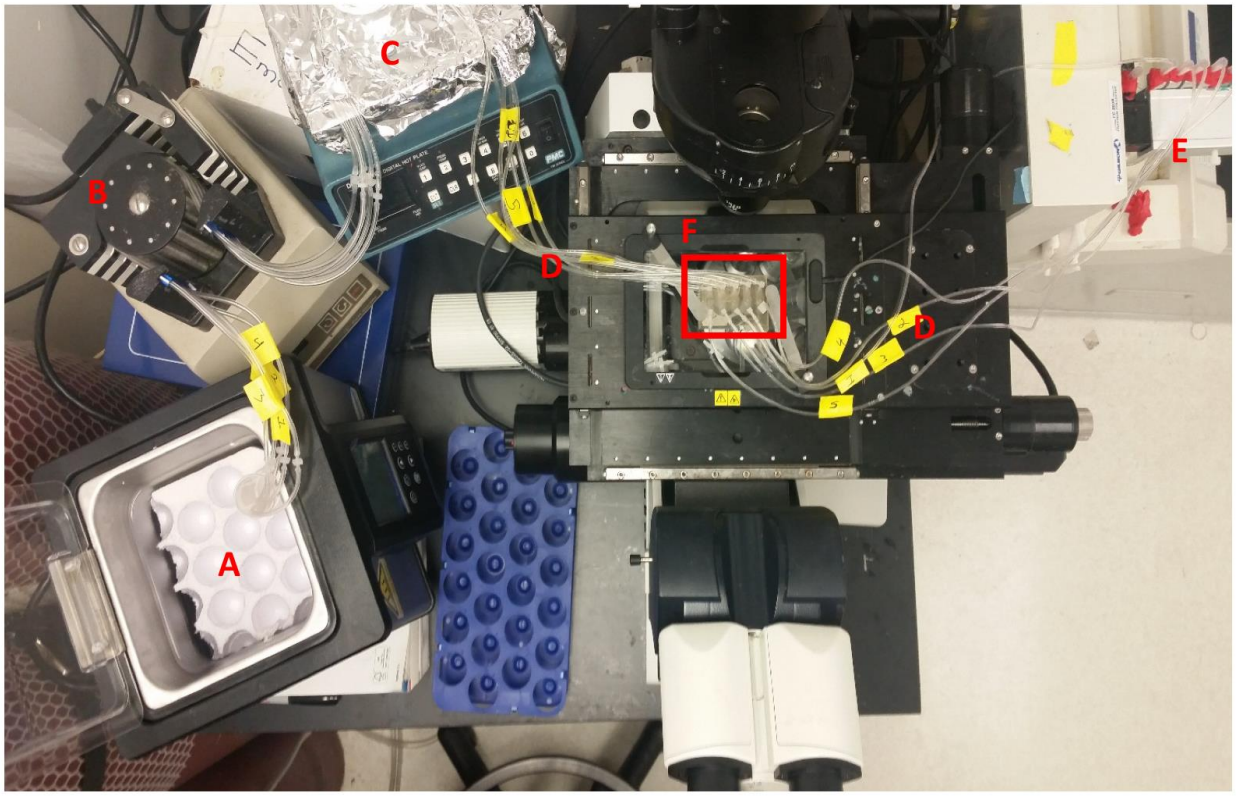

Figure 11. Experimental setup of a typical microfluidic perfusion-based assay on microscope stage. A: Water bath. B: Pump. C: Hot plate. D: Connection tubing. E: Fraction collector. F: Microfluidic device.

2.2 Material and Methods

2.2.1 Device Design and Working Principle

This microfluidic platform is a one-layer poly-dimethylsiloxane (PDMS) device, which has an inlet with radius (Ri) of 1.5 mm and an outlet with radius (Ro) of 7.5 mm (Ro / Ri = 5). The pumpless flow delivery is achieved based on surface tension difference caused by the different diameters of the inlet and the outlet. Between the inlet and the outlet, there is an islet array for holding 20 individual islets based on the hydrodynamic trapping principle, which was first described by Tan and Takeuchi.[59] In two of our previous studies, we have applied the same principle for designing microfluidic devices for islets and microencapsulated islets.[60]

As shown in Figure 12, the channel height is 400 µm and the width is 350 µm, which allows islets to move freely along the channel without causing blockage. The total channel length is around 60 mm with the total liquid volume of approximately 9 µL.

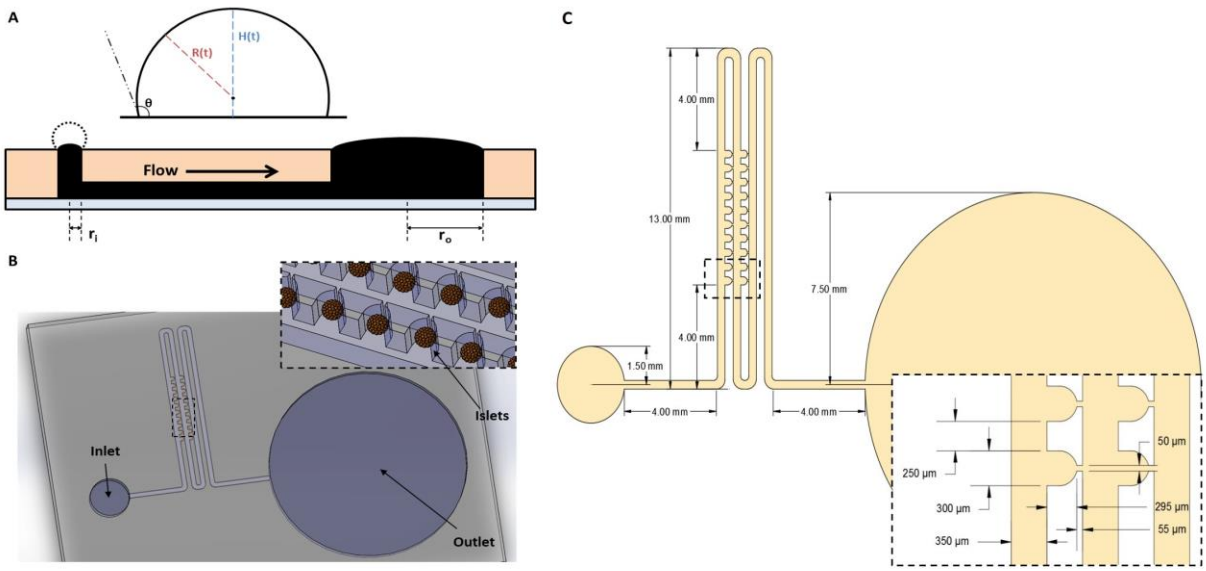

Figure 12. The surface tension driven pumpless microfluidic for islets. A: Working principle of the surface tension driven flow delivery. B: Schematic of the pumpless microfluidic device integrated with islet array. C: Dimension of the surface tension drive pumpless microfluidic.

It has been previously demonstrated that a difference in pressure can be generated between the liquid drop surfaces at an inlet and the outlet of the microchannel due to their different liquid drop diameters.[61] According to the Young-Laplace equation, a smaller curvature radius of liquid drop surface causes a larger pressure, leading to a fluid flow inside the microchannel from a small drop toward a large drop.

In physics, the Young-Laplace equation can be expressed as

$$\Delta P = -\gamma \nabla \cdot \mathcal{n} \text{ or } 2\gamma H \text{ or } \gamma \left(\frac{1}{R_1} + \frac{1}{R_2}\right) \quad (1)$$

Where ΔP is pressure difference across the fluid interface, γ is surface tension, $\mathcal{n}$ is unit normal pointing out of surface, H is curvature, and R is principle radius of a curvature. The equation is a nonlinear partial differential equation that describes the capillary pressure difference maintained across the interface between two static fluids due to surface tension phenomenon. According to the numerical model proposed by the Beebe group, in a microchannel, the gravitational and viscous forces can be negligible since Bo number ($Bo = \rho g R^2/\gamma \approx 0.01$) and capillary number ($Ca = \mu v/\gamma \approx 10^{-4}$) are extremely small and surface tension therefore dominates in driving fluid flow in a microchannel. Since Ro >> Ri (Ro /Ri = 5) in our design, the backward pressure from surface tension of outlet can also be neglected as previously described.[62]

When an inlet drop has radius of R and a surface tension of γ, the Laplace law (pressure difference over an interface in fluid mechanics) can be rewritten as:

$$\Delta P = \frac{2\gamma}{R} \quad (2)$$

In the aforementioned phase model described by the Beebe group, there are three different phases in a droplet evaporation.[63] In the phase I, a droplet starts shrinking on

varying contact angles (from higher contact angle to lower contact angle) but not the drop area. In phase II, droplet area decreases to an equal value of inlet size while contact angle remains the same. In phase III, the contact angle is reduced until the whole droplet disappears. To simplify this model, we adjusted the inlet radius to achieve only the phase III condition, in which the droplet size in the inlet is equal to Ri during the whole shrinking process. It has been shown at room temperature that the contact angle of water on the PDMS surface is about 109º.[64] Therefore, the maximum volume of the drop size is ~13.5 µL with an inlet Ri of 1.5 mm, which means that if drop volume equal to or smaller than 13.5 µL is applied, the droplet wet area will be limited in the inlet port. We applied a 10 µL drop in our later experiments to achieve an efficient stimulation and wash off for the islet cells trapped in the channel since the total volume of the channel is ~10 µL.

For islet immobilization in the microchannel, we designed an array based on the hydrodynamic trapping principle for holding 20 individual islets between the inlet and the outlet. In our previous studies, we have applied the same trapping principle for islets and microencapsulated islets.[60] The islet trapping site is a U-cup shape pocket, superimposed onto a loop channel used for delivering fluid and islets. The U-cup pocket is 250 µm in diameter and 275 µm in depth. There is a cross-flow channel at the apex of the U-cup pocket with a reduction in the width to 45 µm. These design parameters allow capture of 95% of the islet size population.[65]

2.2.2 Computational Simulation of Fluid Dynamics

Two-dimension (2D) computational fluid dynamics (CFD) simulations were performed in COMSOL Multiphysics 5.0 (COMSOL, MA) using a ‘stationary laminar flow’ model. The pressure from surface tension of a 10-µL droplet was applied as the initial

inlet pressure, and both the backward pressure and gravitational force were ignored as discussed previously. No-slip boundary conditions were applied to the walls of the channels. The complete mesh consisted of 60,478 domain elements and 4,033 boundary elements. Error tolerance was 10^{-6}.

2.2.3 Device Fabrication

The device was designed in AutoCAD and printed on a high-resolution (16,000 dpi) transparency film (Fineline Imaging, CO). The device was fabricated based on the method described in 1.2. Specifically, SU-8 2150 photoresist (Microchem, MA) was spun to achieve a thickness of 400 μm for liquid channel, in accordance to the manufacturer's protocol. Following placement of the photomask, the photoresist was then exposed to UV light to polymerize and transfer the pattern to the SU-8. Finally, uncross-linked regions of photoresist were removed by washing the wafer in SU-8 developer solution. Once the SU-8 negative mold master was fabricated, PDMS was poured onto the master to generate a positive mold at the desired thickness. The PDMS mixture was cured for 6 hrs at 80°C. After the PDMS layer was cut and peeled off from the mold, different sizes of punchers were used to puncture inlet and outlet holes for the channels. The PDMS layer and a glass slide were first cleaned with scotch tape, and the two components were then bonded after surface exposure to oxygen plasma and annealed on a hot plate at 80°C for 2 hrs while pressed with a 1 kg weight.

2.2.4 Flow Rate Measurement

Both the average flow rate and the velocity distribution in the microfluidic channel were measured to characterize the device. The average flow rate was determined by recording the drop shrinking process using a high-speed camera (iPhone 5s, custom

Sony Exmor RS, 720p slow-motion video at 120 fps). Time course for the delivery of the 10 µL drop was determined by examination of the movie frame by frame (each frame is ~0.008 second when recorded at 120 fps mode), and the flow rate was calculated based on volume over time. The micro particle image velocimetry (µ-PIV) technique is often applied to obtain micron-resolution velocity measurements in microscale channels.[66] In this study, the microscale fluorescent particles (Fluospheres polystyrene microspheres, 1.0 µm, red fluorescent 580/605, Thermo Fisher Scientific Inc.) acted as a flow tracer in our simplified µ-PIV for the velocity measurements of surface tension driven flow in the channel. The distance of bead movements in different areas of the channel were recorded by measuring the tracing lines of the beads under 4-ms exposure time using a charge-coupled device (CCD, Retiga-SRV, Fast 1394, QImaging), and the velocity of individual particles was then calculated from the locus.

2.2.5 Islet Isolation and Preparation

Mouse pancreatic islets were isolated from the pancreata of 10 to 12-week-old C57/B6 mice (Jackson Laboratory, MA) and cultured according to the established methods. In brief, as shown in Figure 13, the pancreata were injected with 0.375 mg/mL of Collagenase P (Roche Applied Science, IN) and then digested at 37 °C for 15 min. Islets were purified through a discontinuous Ficoll gradient (Mediatech, VA) and then cultured in RPMI 1640 medium supplemented with 10% fetal bovine serum (Hyclone Inc., MA) and 1% penicillin/streptomycin (Mediatech, VA) at 37°C under 5% CO_2.

Human islets were provided by human islet isolation team from Chicago Diabetes Project.

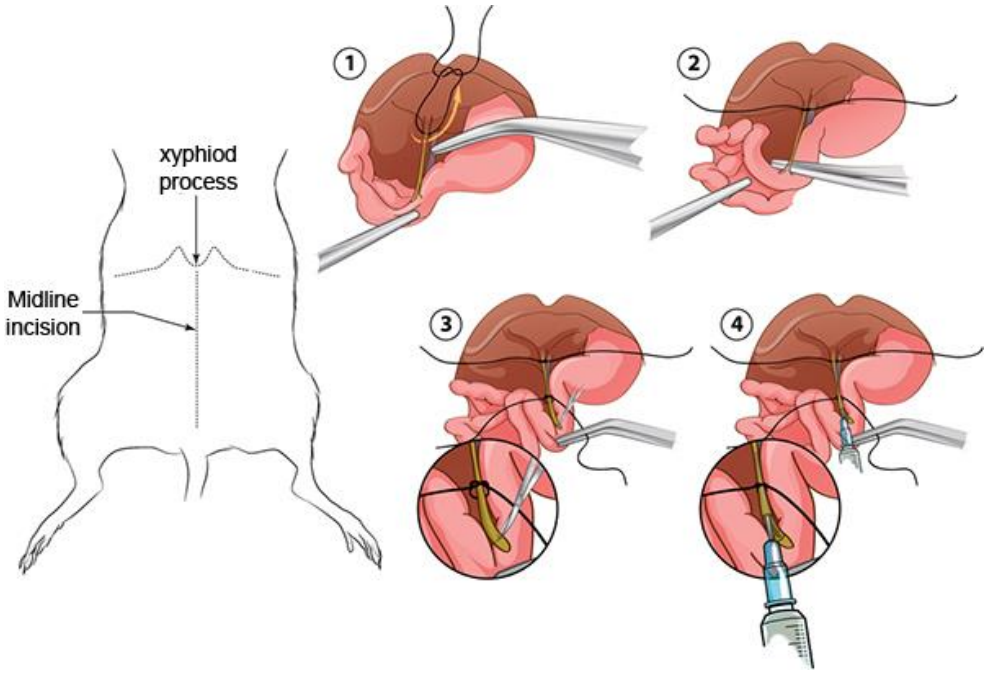

Figure 13. Enzyme injection steps for mouse islet isolation. Adopted from reference [67].

2.2.6 Buffer Solutions and Islets Loading

All insulin secretagogues were prepared in Krebs Ringer buffer (KRB): 129 mM NaCl, 5 mM $NaHCO_3$, 4.7 mM KCl, 1.2 mM KH_2PO_4, 1 mM $CaCl_2 \cdot 2H_2O$, 1.2 mM $MgSO_4 \cdot 7H_2O$, 10 mM HEPES, 2 mM basal glucose, and 5% FBS at pH 7.35-7.40. Fura-2 AM for calcium imaging was prepared in DMSO and Rh123 for determining mitochondrial potentials was prepared in 100% ethanol at final concentrations of 5 μM and 2.5 μM, respectively. Islets were loaded into the trap area through a pipette tip connected at an inlet by gravity.

2.2.7 Fluorescence Imaging and Insulin Collection

A schematic experimental setup is depicted in Figure 14. All imaging experiments were conducted according to previously described methods.[57] For the entire procedure, a 10 μL pipette was used to drop a consistent volume of liquid. 10 droplets of the KRB containing 2 mM glucose were first applied to wash excess fluorescence. The KRB containing high glucose (14 or 25 mM) or KCl (30 mM) was then administered to stimulate the islets, and the fluorescence signals were recorded with imaging software (HCImage, Hamamatsu Photonics, Japan). The $[Ca^{2+}]_i$ of Fura 2-loaded islets was indicated by the ratio of 340- and 380-nm excitations, and the 340/380 ratio changes were then converted to percentage changes. Raw baseline of Fura-2 was about 0.4 in KRB with 2 mM glucose. Meanwhile, raw basal intensity of Rhodamine 123 was around 200 (au). Perifusate samples were collected at the outlet every 2 minutes for later insulin determination. The dilution ratio was 1/10 and was achieved by diluting 10 μL sample in 90 μL deionized water.

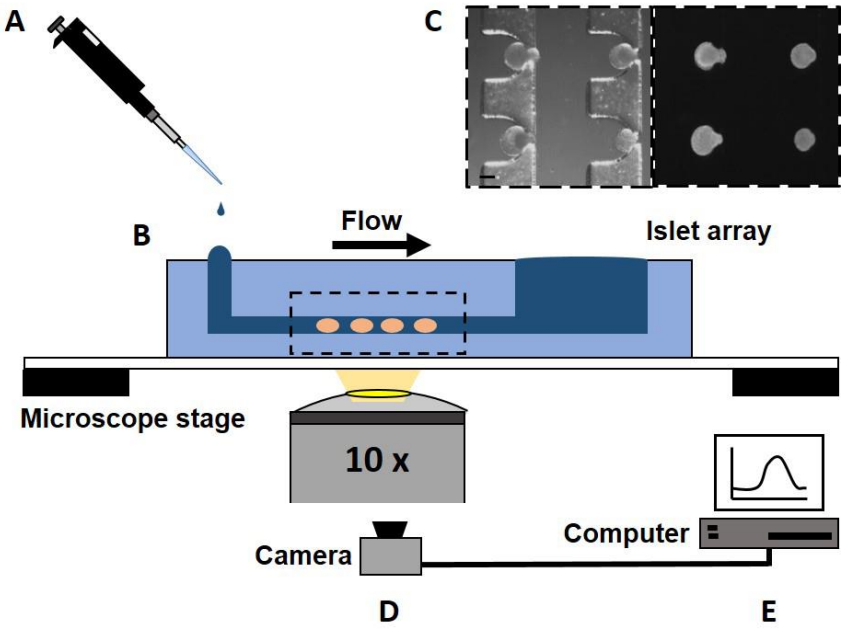

Figure 14. Schematic of experimental setup. A: Flow delivery. B: Microfluidic device. C: Islet array. The scale bar in the figure is 100 μm. D: Microscope and data collection. E: Data Analysis.

2.2.8 Insulin ELISA

Insulin concentrations were measured using Human or Mouse Insulin ELISA kits (Mercodia AB, Uppsala, Sweden) according to provided protocols using Biotek Synergy 2 microplate reader (BioTek U.S., Winooski, VT).

2.3 Results and Discussion

2.3.1 Flow Characterization

The computational simulation of flow velocity before the islet trapping pocket was conducted using the COMSOL Multiphysics as shown in Figure 15A. Only an initial flow rate was measured since flow rate would slightly decrease during the process of droplet shrinking. However, it would not affect the efficient flow delivery and exchange to islets since it takes less than 4 seconds. The velocity profile in the area was shown to be bell-shaped. The center of the channel had the highest flow velocity at 23.5 mm/s when Ri was 1.5 mm and Ro was 7.5 mm.

To confirm the pressure generated by surface tension, we further compared the simulation results with experimental results using fluorescence beads. Our results showed that there was an extreme similarity on the distribution of initial velocity (Figure 15B). At the center of the channel, highest flow velocity (~ 23.5 mm/s) was noted, with a similar velocity to the simulation result. The polynomial trend lines showed that in general, the experimental results were slightly higher than the simulation results. The small difference could be explained by the fact that the simulation was a 2D model while the experimental condition was 3D, in which islets or beads could not completely block the flow, which resulted in a slightly higher flow velocity in the trapping pocket. In the area close to the channel wall, the velocity in the experimental results was higher than the

simulation results (2.5 mm/s vs. 0 mm/s), which was caused by ignorance of friction and viscose effects in the computer simulation, especially at the near-wall area, for simplifying the numeric modeling and calculation.

Since the distance between the inlet and the islet trap site was approx. 8 mm, it would be expected that flow takes approximately 0.3 seconds from the inlet port to the cells trapped in the array. It is noted that the flow rate is not consistent with slight decrease over time; however, the slight flow rate decrease would not have a significant negative impact for live-cell imaging since flow takes less than 1 second from the inlet port to the islets trapped in the array. For application in long-term cell culture, it would be ideal to integrate an automate flow dispenser such as a droplet replenishment system to keep continuous flow and consistent flow rate.

Complete flow exchanges in the device would take approximately 2.5 seconds based on the computer simulation and experimental results. The rate of solution exchange was significantly faster as a result of small channel size and volume in comparison to our previous perifusion chamber design, which required 3 minutes to achieve a complete flow exchange.[68] Therefore, the device acts as a super-efficient stimulation platform for studying islet physiology.

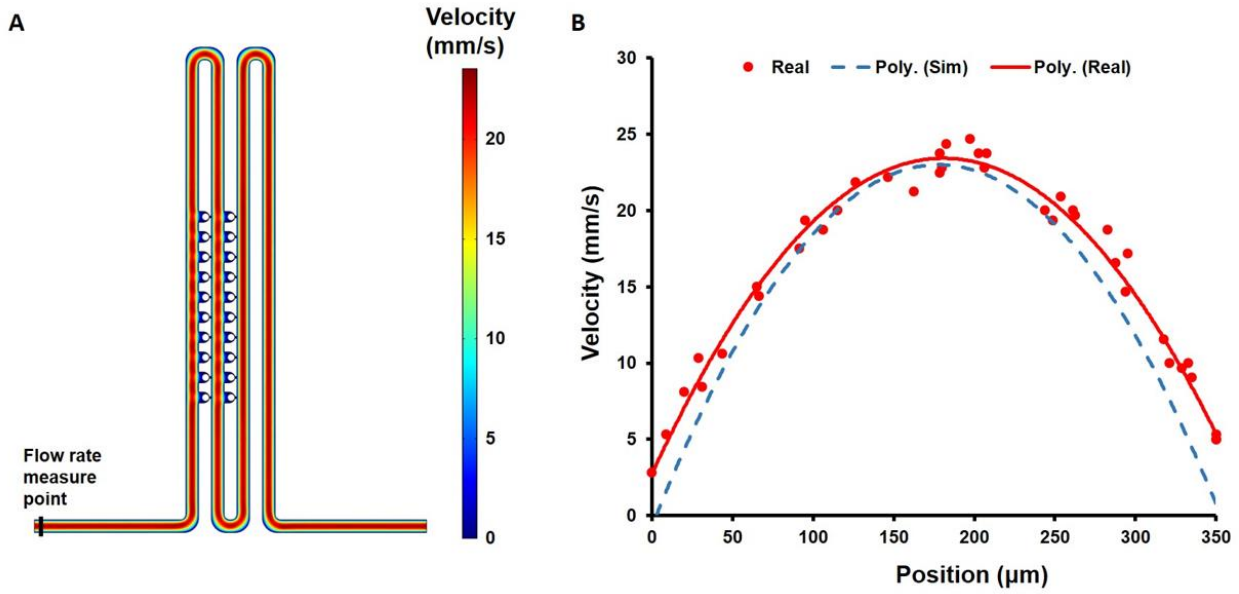

Figure 15. Flow rate characterization. A: The computational simulation of flow-rate. The flow rate measure point is labeled at the beginning of the channel. B: The initial velocity distribution in the channel at the measure points compared with computational simulation results. X-axis represents the position on the cross-section direction from the left wall (0 μm) to the right wall (350 μm) of the channel. N = 3.

In order to serve specific experimental requirements, flow speeds could be adjusted by designing different Ri/Ro. As described previously, the flow rate was dependent on the size ratio of the inlet and outlet and when Ro >> Ri, the backward force could be neglected due to the much smaller pressure produced from surface tension of the large droplet. To confirm this, we designed five devices with different Ri/Ro ratios (1:1, 1:2, 1:3, 1:4, and 1:5) and flow rates were then compared.

As shown in Figure 16, in the device that had the same sized inlet and outlet, no fluid flow was observed due to the same pressure generated from the identical drop size, which also proved that the gravitational effect was negligible. The average flow rates were increased by enlarging the dimension difference between Ri and Ro, indicating that the flow rates were 6.11 μL/s ± 0.30 for Ri/Ro of 1:2, 8.82 μL/s ± 0.59 for Ri/Ro of 1:3, 11.86 μL/s ± 0.40 for Ri/Ro of 1:4, and 14.44 μL/s ± 0.37 for Ri/Ro of 1:5. In conclusion, the higher Ri/Ro gives a faster delivery of fluid until the backward pressure could not be neglected any more compared to the driving force from the inlet.

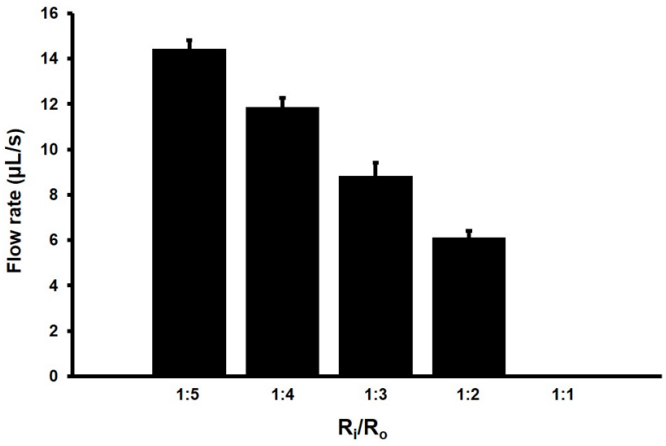

Figure 16. Varying flow rates achieved by different diameter ratios of inlet and outlet. Data were expressed as mean ± SD. N = 3 for each ratio.

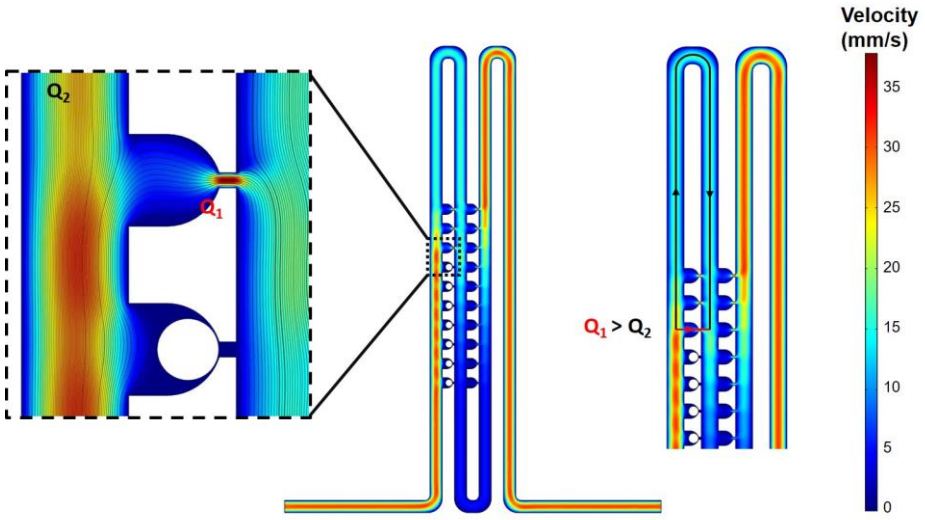

Figure 17. Flow dynamic simulation in the microfluidic islet array. The average flow rate in the neck of the U-cup trapping area is labeled as Q1, and that of the loop channel is labeled as Q2. The circular blocks are used to mimic the loaded islets in the first several traps.

2.3.2 Islet Trapping Mechanism

Islet immobilization was achieved using a hydrodynamic trapping mechanism first described by the research group Tan and Takeuchi. The islets were trapped based on the flow resistant difference between the U-cup and the loop channel. When flow carries an islet to the junction between the U-cup (trapping area) and the loop channel, an islet will be trapped in the U-cup due to less resistance. The trapped islet results in increased resistance in the U-cup and the flow is then redirected into the loop channel. This flow carries subsequent islets towards the next empty U-cup, iterating the trapping downstream throughout the device. Flow dynamic simulation is shown in Figure 17, and indicates that the trapping area has lower flow resistance and higher flow velocity (Q1) than the loop channel (Q2), which results in particle movement into the trapping area when the U-cup is empty. Combined effects of these two flow forces determine the trapping efficacy of individual islets. The optimal geometry for trapping efficacy was determined by testing varying lengths, widths, and depths of the trapping site and the loop channel in computational simulation with COMSOL Multiphysics, and was further verified in our previous study.[13]

2.3.3 Effect of Shear Stress on the Trapped Islets

In previous studies, it has been shown that sheer force from fluid flow in the microfluidic channel may cause an influx of calcium ions in human endothelial cells.[69] Considering the possible effect of sheer force on the trapped islets in our design, we studied calcium influx during the continuous dropping of 2 mM glucose solution with and without calcium ions in Krebs-Ringer buffer, and $[Ca^{2+}]_i$ was then continuously monitored. Figure 18A and 18B represent the $[Ca^{2+}]_i$ of mouse and human islets in response to

continuous dropping of 2 mM glucose with and without calcium, and show no obvious correlated response of $[Ca^{2+}]_i$ to the increasing flow rate from the drops and minimal overall increase in $[Ca^{2+}]_i$. These results indicated that the intracellular calcium ion generated from the sheer flow was very limited in our device.

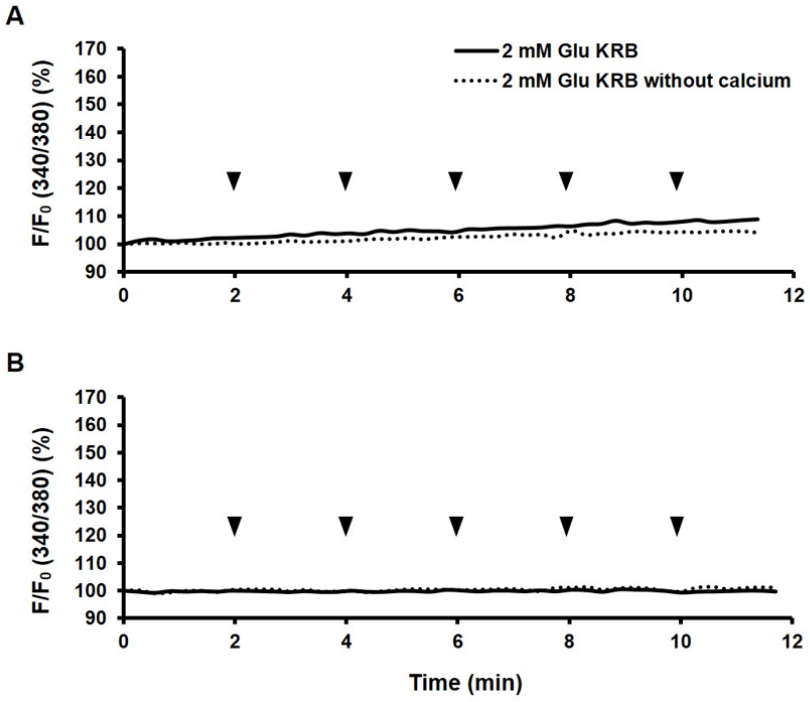

Figure 18. Effect of flow shear stress on trapped islets. A: Representative trace of rodent islet calcium signaling in response to continuous dropping of 2 mM glucose with and without Ca^{2+}, and the drops are indicated by the black arrows. N = 3. B: Representative trace of human islet calcium signaling in response to continuous dropping of 2 mM glucose with and without Ca^{2+}, and the drops are indicated by the black arrows. N = 3.

2.3.4 Perifusion and Fluorescence Imaging of Rodent Islets

As shown in Figure 19A and 19B, the $[Ca^{2+}]_i$ of isolated rodent islets increased up to 170.08% ± 14.69 in response to 14 mM glucose with a total liquid consumption of 60 µL over a 10 min stimulation period. The increased $[Ca^{2+}]_i$ occurred after 2.39 min ± 0.06 post glucose stimulation and showed a typical biphasic profile that is a very important signature of islet calcium signaling for stimulation and regulation of efficient insulin secretion. Importantly, the device design improved the precision and sensitivity of islet calcium signaling by effectively detecting subtle changes such as phase 0, which is often not detectable in our previously designed perifusion based device.[68] The glucose-induced phase 0 is a gradual depolarization of the cell membrane and a decrease in intracellular calcium levels. A lack of (non-detectable) phase 0 is often caused by endoplasmic reticulum stress associated with a defect in islet cell function.[70] Similarly, the rodent islets had intracellular calcium increase of 210.88% ± 21.17 in response to 30 mM KCl stimulation. The time to reach peak post stimulation is 1.60 min ± 0.06.

The increases of $[Ca^{2+}]_i$ in response to 14 mM glucose and 30 mM KCl could be reduced to near basal levels (<120%) when the islets were washed with 2 mM glucose without a significant delay time (6.27 min ± 0.06 for glucose and 3.61 min ± 0.06 for KCl, respectively), indicating an efficient flow exchange in the pumpless device. Perifusion experiments using mouse islets were also performed in our traditional microfluidic perifusion chamber device for comparison (data not shown).[57]

Similar to nerve and many endocrine cells, beta-cells within islets are electrically excitable, producing electrical impulses in response to glucose challenges. The electrical spiking pattern typically comes in the form of bursting, characterized by periodic clusters

of impulses followed by silent phases. The bursting electrical activity is critical since it leads to oscillations in the intracellular calcium concentration, which in turn leads to oscillations in insulin secretion.[71] In general, there are two distinct calcium oscillation patterns: fast oscillations (1-2 min) and slow oscillations (4-6 min). Calcium oscillations appear to be the driving mechanism behind pulsatile insulin secretion. In fact, coherent insulin and calcium oscillations are disturbed or lost in patients with T2DM.[72, 73] As shown in Figure 19C, isolated rodent islets started calcium oscillations after 10 min in response to 14 mM glucose, which indicates a slow oscillation (3.15 min/cycle ± 0.54). The perifusate samples were collected and insulin secretion levels were determined using ELISA as shown in Figure 19D. Similar to the $[Ca^{2+}]_i$ signaling, insulin secretion also showed typical biphasic profiles with a peak concentration of 14.86 ng/mL ± 1.60 for 20 islets in response to 14 mM glucose stimulation.

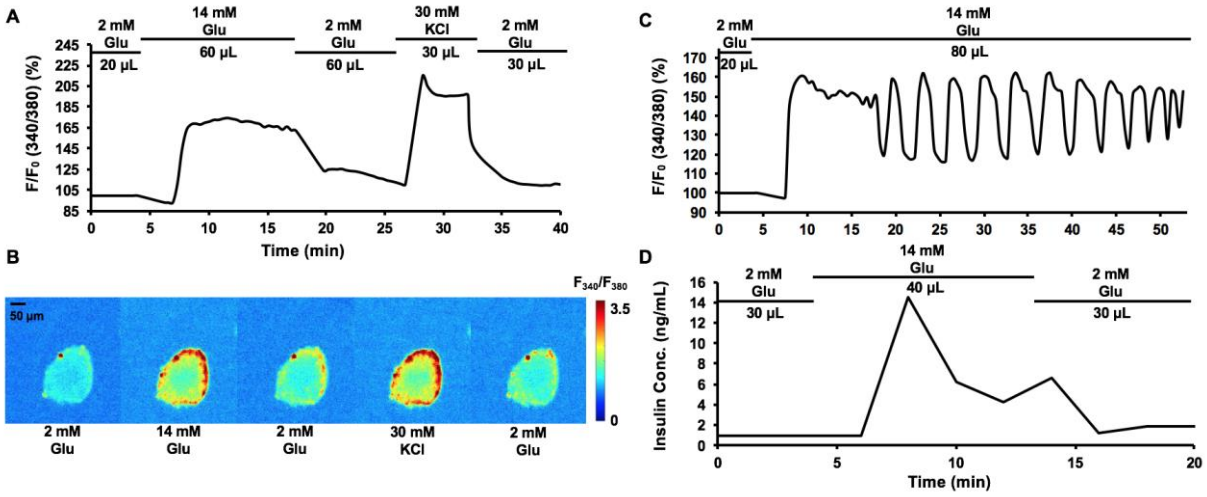

Figure 19. Perifusion and imaging of rodent islets. A: Representative trace of rodent islet calcium signaling in response to 14 mM glucose and 30 mM KCl. N = 50 - 60 islets from three independent islet samples. B: Images of Fura 2 340/380 in corresponding to each stimulation phase. C: Representative trace of rodent islet calcium oscillation in response to 14 mM glucose. N = 50 - 60 islets from three independent islet samples. D: Representative trace of rodent islet insulin secretion in response to 14 mM glucose N = 3.

2.3.5 Perfusion and Fluorescence Imaging of Human Islets

Allogeneic islet transplantation is a promising cell-based therapy for Type I diabetes patients; however, it often results in varying rates and duration of insulin independence.[74-76] One of the primary reasons underlying such variations in insulin independence is the inconsistent or undefined quality of human islets transplanted in patients. In our previous study, we developed a microfluidic-based multiparametric assay for functional characterization of the human islets by the simultaneous measurements of insulin secretion and the key insulin stimulator-secretion coupling factors, such as intracellular calcium flux and mitochondrial potential. Calcium signaling can be used to detect differences in the function of human islet preparations and exhibits a strong predictive power for a given human islet preparation to cure diabetes (data not shown). However, the glucose and KCl induced insulin secretion kinetics of isolated human islets have less predictive values. A possible reason for this might be related to the large volume of the perifusion chamber (115 µL) and the perifusate volume (250 µL/min) that reduces the sensitivity of the assay, especially when lower amounts of insulin are secreted. Furthermore, the syringe-based flow delivery system can cause flow fluctuations and inhomogeneous flow mixing. In this study, an islet array integrated with the surface tension-driven pumpless flow delivery system reduced total device volume from 115 µL to 10 µL and perifusate volume from 250 µL/min to 20 µL/min, which may be helpful for providing better spatiotemporal resolution of insulin secretion kinetics in future.

As shown in Figure 20A and 20B, $[Ca^{2+}]_i$ levels of human islets increased by 142.77% ± 9.60 and 185.01% ± 3.54 in response to 25 mM glucose and 30 mM KCl, respectively. Mitochondrial potential changes dropped to 97.27% ± 1.47 in response to

the glucose stimulation shown in Figure 20C. Both calcium signaling and mitochondrial potential changes were comparable to our perifusion chambers. In Figure 20D, the insulin secretion in response to insulin stimulators also showed a biphasic profile with a peak concentration of 16.11 ng/mL ± 0.25 for 20 islets in response to 25 mM glucose stimulation and 36.19 ng/mL ± 1.79 in response to 30 mM KCl.

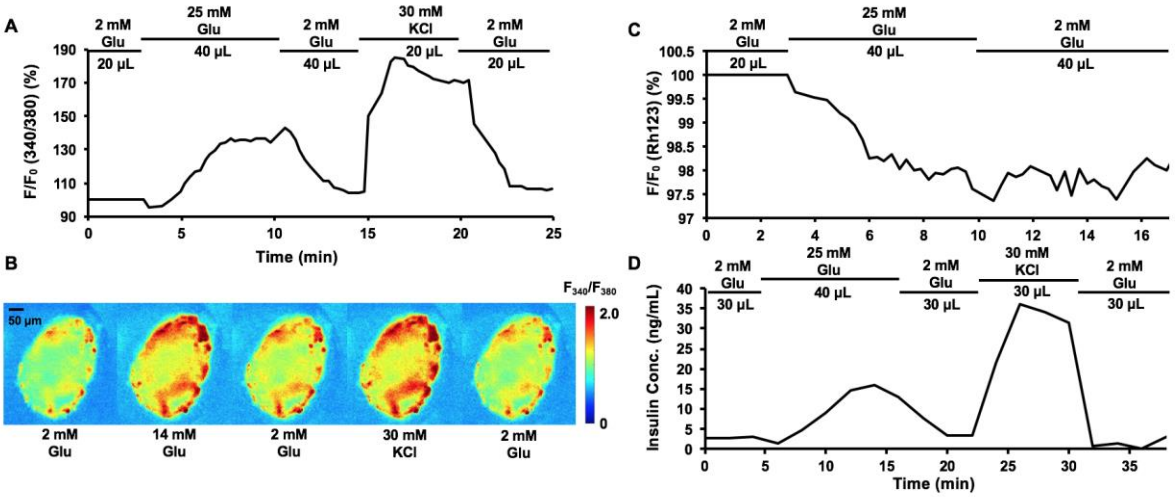

Figure 20. Perifusion and imaging of human islets. A: Representative trace of human islet calcium signaling in response to 25 mM glucose and 30 mM KCl. N = 50 - 60 islets from three independent islet samples. B: Images of Fura 2 340/380 in corresponding to each stimulation phase. C: Representative trace of human islet mitochondrial potential changes in response to 14 mM glucose. N = 50 - 60 islets from three independent islet samples. D: Representative trace of human islet insulin secretion in response to 14 mM glucose and 30 mM KCl. N = 3.

2.4 Conclusion

In this study, we presented a novel pumpless islet microfluidic device based on the forces driven by surface tension in a self-designed microfluidic. The fluid flow dynamics were characterized by both computer simulation and experiments. High-resolution analysis of individual rodent and human pancreatic islets was also performed in the hydrodynamic trapping array area. This work indicated the possibility of eliminating the pump and tubing from the set-up of most islet microfluidic devices, and also the capability of quantitative analysis of islet physiology. In contrast to existing islet microfluidic perifusion devices, the presented pumpless platform provides opportunities for faster fluid delivery, more efficient stimulation to islets, and less solution consumption with improved spatiotemporal resolution of the parameters measured. One limitation of the system is that only one flow rate can be achieved for one working device at the present moment; however, varying flow rate devices can be easily designed based on the same design principle and have been demonstrated in the aforementioned results. A single device with integration of varying flow rates is under investigation.

Herein, the presenting microfluidic platform can be utilized in future studies of islet physiology and pathophysiology, evaluation of human islet function and viability prior to human islet transplantation for Type I diabetes patients, antidiabetic drug development, and stem cell characterization. Importantly, the removal of the pump set-up and accessories is meaningful at a practical point of view for developing a microfluidic islet device for a broad laboratory application.

3. MICROENCAPSULATION OF PARATHYROID CELLS IN MICROFLUIDIC CHANNELS

3.1 Introduction

3.1.1 Parathyroid Glands and Hormone

The human parathyroid glands are four tiny glands of the endocrine system which are located in the cervical region behind the thyroid. They mainly control calcium and phosphate metabolism in our bodies through the secretion of parathyroid hormone (PTH). Each gland is about 3-4 millimeters wide, and weighs approximately 30 milligrams, with a similar appearance of a lobule of the thyroid gland.[77] Therefore, the thyroidectomy frequently results in the accidental removal of the parathyroid glands and cause hypoparathyroidism. Like liver tissue, a small amount of parathyroid tissue is sufficient to provide enough function, so removal of even three of the four glands would cause only transient hypoparathyroidism.[78]

The adult human parathyroid gland has two cell types: chief cells and oxyphil cells. Chief cells are responsible to secrete PTH to regulate blood calcium level. On the other hand, there is evidence of transitional oxyphil cells showing that oxyphil cells derive from chief cells that no longer secrete hormone during aging.[79] Additionally, oxyphil cells are larger than chief cells (12-20 μm vs. 6-8 μm), but their function is unknown. Another evidence for transition of a chief cell to oxyphil cell is that both transitional and oxyphil cells express PTH and Glial Cell Missing 2 (GCM2), an essential transcription factor in parathyroid gland development.[79]

The parathyroid gland has remarkably high sensitivity to sense minor changes in blood serum concentration of calcium ion, and regulates hormone synthesis and secretion immediately as response. When the low blood calcium level is detected by glands, parathyroid chief cells produce and secret PTH to increase the amount of calcium in the blood. Conversely, when the calcium level in the blood is too high, PTH secretion from parathyroid cells is inhibited, leading to a lower calcium level. Therefore, benefit from this feed-back mechanism, blood serum Ca^{2+} and PTH level are maintained in a narrow range.[80]

PTH is synthesized from chief cells as a polypeptide chain of 110 amino acids at beginning, and then being cleaved and matured itself to 84 amino acids. The final PTH molecule, which is delivered in secretory granules like insulin in beta cells, has a molecular weight of approximately 9.5 kDa. However, a smaller peptide isolated from the parathyroid glands with only 34 amino acids adjacent to the N terminus of PTH molecule showed functional active.[81]

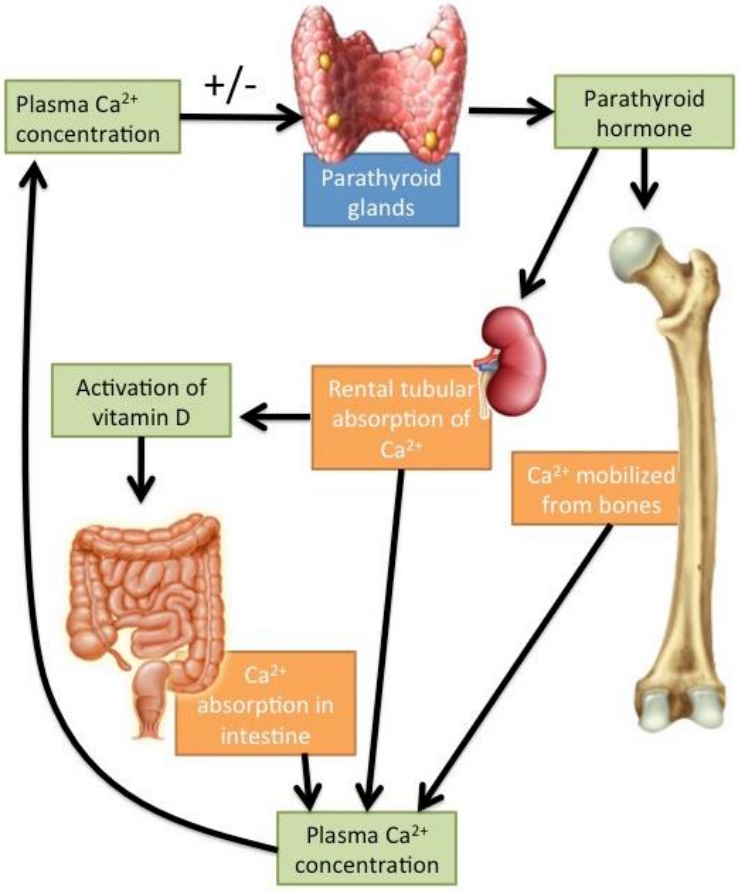

Figure 21. Functions of PTH in maintaining calcium balance. Adopted from http://ouopentextbooks.org/biol3103/author/kbrown/.

As illustrated in Figure 21, PTH can increase plasma Ca^{2+} concentration via three different mechanisms:[81]

a) In bone, PTH has biphasic effect to enhance the release of Ca^{2+} and phosphate. Due to the activation of the osteocytes to promote Ca^{2+} reabsorption, A rapid phase begins immediately after PTH kicks in and causes dramatic increase of calcium mobilization from bones within several hours. However, it is much slower to release calcium in the second phase, which often takes days or even weeks. The proliferation of the osteoclasts and subsequently increased osteoclastic reabsorption of the bones are the reason behind the slow phase.

b) In kidney, PTH increases renal tubular reabsorption of Ca^{2+} at distal tubules and the renal collecting ducts, and meanwhile, inhibits the reabsorption of phosphate from the tubular fluid. Consequently, phosphate concentration decreases, and thus, for a given total calcium concentration, this further increases the Ca^{2+} concentration in plasma. Another important effect of PTH on the kidney is to trigger the conversion of 25-hydroxy vitamin D into 1,25-dihydro vitamin D, which is involved in PTH function in intestine.

c) In intestine, as described above, PTH enhances both Ca^{2+} and PO_4 reabsorption by increasing the production of activated vitamin D in the kidney.

3.1.2 Hypoparathyroidism

Hypoparathyroidism is a rare endocrine disorder associated with extremely low serum calcium and increased serum phosphorus due to is abnormally low or no PTH production. [82] Based on data from National Organization for Rare Disorders (NORD), the prevalence of hypoparathyroidism in the general population 37 per 100,000 person-years in the US. Hypoparathyroidism can affect individuals of any age.

As summarized in Table 1, hypoparathyroidism most common cause is surgical removal of the parathyroid glands. Partial damage or complete removal of gland tissue or blood supply often happens in surgical treatment for other conditions, like hyperparathyroidism or cancer of thyroid. Post-surgical reasons cause 78% of cases of hypoparathyroidism.[83] In rare cases, hypoparathyroidism occurs as an autoimmune disorder. Autoimmune hypoparathyroidism can be part of a larger autoimmune syndrome that damages multiple organs of the body or as sole target of autoimmune attack. There are other common causes that need to be ruled out including hypo-magnesemia or hyper-magnesemia, which are often reasons of pseudo-hypoparathyroidism. Magnesium is involved in the secretion of PTH in parathyroid cells, so either its depletion or excess may cause hypoparathyroidism and subsequent hypocalcemia. The reason behind this is that magnesium concentration can affect cyclic AMP formation in parathyroid chief cells and thus interfere with PTH synthesis and secretion.[84] Congenital hypoparathyroidism patients are born without functional parathyroid glands or have an isolated genetic disorder. Examples of the more common genetic causes of hypoparathyroidism are mutations of the extracellular calcium-sensing receptor (CASR) or G-alpha 11 gene, which leading to suppression of parathyroid hormone secretion.

MECHANISM	*COMMENT*
Destruction of parathyroid tissue	
Postsurgical	Most common form of hypoparathyroidism
Postradiation	Rare complication
Autoimmune	May be associated with other endocrine insufficiencies
Metastatic infiltration	Case reports
Heavy metal deposition	Iron deposition in 10% of persons with thalassemia
Reversible impairment in parathyroid hormone secretion or action	
Hypomagnesemia	Chronic illness, drugs, acidosis
Hypermagnesemia	Tocolytic therapy, magnesium supplementation
Resistance to parathyroid hormone action	
Pseudohypoparathyroidism	—
Genetic disorders of parathyroid hormone synthesis	

Table 1. Common causes of hypoparathyroidism.

Symptoms of hypoparathyroidism are caused by effects of low serum calcium on the internal organs. Although symptoms may varied between individuals, they can include muscle aches or cramps, tingling, muscle twitching or spasms, painful menstruation, patchy hair loss, low blood pressure, seizures and heart failure.[85] In most patients, symptoms appear when the albumin-corrected serum calcium concentration is lower than 7.5 mg/dL.[78]

Careful surgery on patients with hyperparathyroidism will reduce the risk of postsurgical damage to further cause parathyroid gland dysfunction. In addition, re-implantation of some parathyroid tissue can reduce postoperative damage after an extensive surgery of thyroid is performed. Pre-surgical optimization of vitamin D is also helpful, since vitamin D deficiency often happens in cases of parathyroid surgery. Conventional vitamin D therapy uses vitamin D or its analogs to increases intestinal calcium absorption and subsequent blood serum calcium levels, but renal calcium reabsorption is still low and often cause excessive urinary calcium excretion. Such chronic hypercalciuria without specific treatment can lead to nephrocalcinosis, renal impairment and insufficiency. The bovine PTH was attempted to use to treat hypoparathyroidism and failed due to the adapted resistance. The synthetic PTH (34 amino acids) has been investigated in many studies and showed positive results in short-term. In long-term, safety control is necessary before they can be applied to potentially reduce the need for calcium and vitamin D supplements in hypoparathyroidism patient treatment. In 2015, FDA approved the recombinant human PTH, the first approved form of PTH with 84 amino acids, for adjunctive therapy in management of hypoparathyroidism in patients not treated

with calcium, magnesium, vitamin D therapies as needed. But there was increased risk of hypercalcemia reported in US trials. [86-89]

While PTH replacement has not shown to be effective and clinically safe, allotransplantation of parathyroid cells was proposed as a therapeutic alternative.[90] However, it needs an immunosuppressant, which often evokes many complications. A promising method to overcome graft rejection and immunosuppression is encapsulation of parathyroid cells.[91]

3.1.3 Cell Encapsulation

Cell microencapsulation is a technology for cell immobilization in productions of cell-therapeutic product. In general, cells in microcapsules are surrounding by a polymeric semi-permeable membrane, which can protect the encapsulated cells from rejection attack of host immune system after implant, and meanwhile, allow bidirectional diffusion of molecules essential for cell metabolism or secretory products, such as the oxygen, nutrients, growth factors, and hormones.[92]

One advantage of using the microencapsulation technique is that the encapsulated cells would provide a more sustainable source compared to naked implant tissue to continuously release therapeutic products in long-term and thus potentially achieve functional cure of diseases. Another advantage of cell microencapsulation technology is that it allows the implant of encapsulated non-human and genetically modified cells without strong activation of host immune system.[92] Microencapsulation technique is extremely valuable not only because it can provide the prolonged delivery of therapeutic products to the target site, but also it would be more cost effective in comparison to direct drug injection to implant these artificial cells.[92]

The method of islet encapsulation by using a semi-permeable membrane to protect cells from the recipient immune response was established in 1970s and has been applied since then. However, in rodent models, results varied from cases conducted in both academic and industrial facilities. These results from non-human models and initial clinical trials suggested there is still a long way to go in proving non-immunoreactive encapsulation method.[93] As shown in Figure 22, a typical encapsulated islet is enveloped by a porous membrane, which allows passage of oxygen, glucose, nutrients and secretion of insulin.[94]

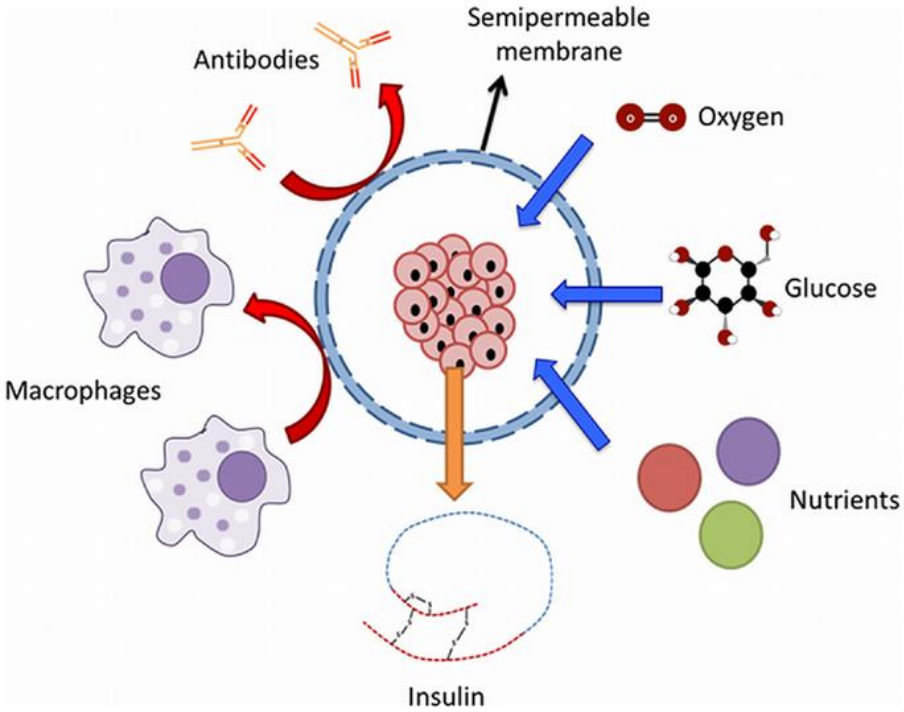

Figure 22. Schematic representation of microcapsules for pancreatic islets.

Adopted from reference [94].

The optimize multiple variables affecting cell microencapsulation for a successful clinical application, first thing is choosing proper capsule materials based on their mechanical and chemical stability, biocompatibility and biodegradability, polymerized matrix permeability. In addition, sizes and shapes of capsules are also crucial in speaking of cell function and survival after implant, due to the consequently affected diffusion efficiency of molecules. Several research groups have reported their studies about natural and synthetic polymers that can be used for cell microencapsulation.[95, 96] From extensive previous work by researchers, it has been demonstrated that alginates are the most suitable biomaterials for cell encapsulation in the application of transplant due to their abundance and excellent biocompatibility and biodegradability. Alginates, natural polymers which are extracted from various kinds of seaweed and bacteria, are a family of unbranched binary copolymers of 164 linked β-D-mannuronic acid (M) and a-L-guluronic acid (G).[97] By adding certain concentration of ions, alginates will be polymerized and form gels. However, the rigidity alginate gels varies when adding different ions and increases with the affinity of the ion in the order: Mn > Co > Zn > Cd >Ni >Cu > Pb > Ca > Sr > Ba.[98] Since most of these ions cannot be used for immobilization of therapeutic active cells due to their cytotoxicity, Ca^{2+} is commonly chosen for alginate gelation in cell microencapsulation.

Traditionally, the immobilization of cells in alginate gels to create alginate-based microcapsules relies on an electrostatic droplet generator. Such an encapsulation system consists of an electrostatic droplet generator and a tunable peristaltic pump. As shown in Figure 23, initially, cells are suspended in alginate solution, and delivered by external pump to a tiny tip to be extruded using the electrostatic device. Because only $CaCl_2$ is

used as gelation solution, beads with inhomogeneous cores will be formed. The addition of NaCl will result in homogeneous core beads.[94] However, due to the complexity of setup of multiple variables, it shows difficulty in size control, encapsulation efficiency, and cell positioning.

Microfluidic platform offers a unique advantage in generating uniform-sized emulsion droplets, with tunable size ranging from a few to hundreds of microns. Homogeneity can be seen in particle size as well as cell distribution inside the particle, leading to more sustained biomolecule penetration and cell viability. Bypassing the filtration step also increases the overall yield of production.

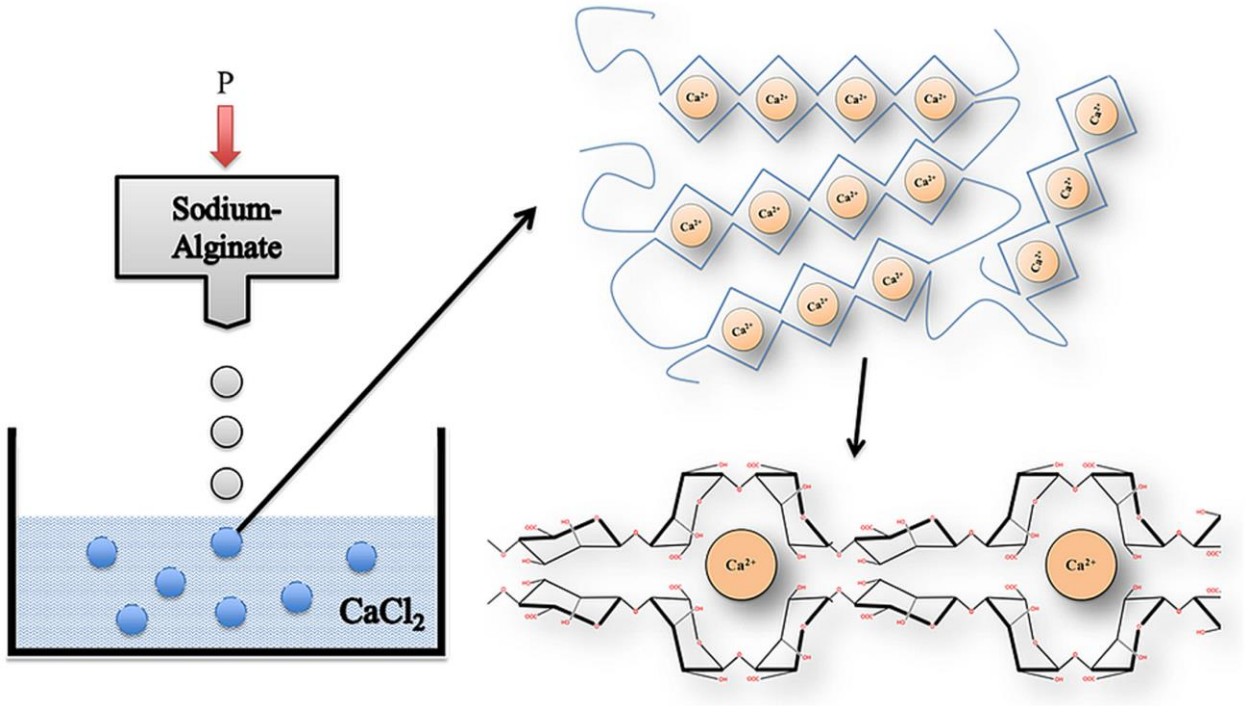

Figure 23. Gelation process of alginate in cell encapsulation. Alginate dropped from an air droplet generator into a $CaCl_2$ solution to form a non-homogenous microcapsule. Gels are formed by cross-linking of alginate-polymers with calcium ions between G-G and M-G-blocks. Adopted from reference [94, 99].

3.2 Materials and Methods

3.2.1 Design Idea and Microencapsulation Principle of Device

Researchers have been using a technique called “flow focusing” to produce drops or bubbles by straightforward hydrodynamic means in microfluidic channels. The basic principle consists of a continuous phase fluid (focusing or sheath fluid) surrounding the dispersed phase (focused or core fluid), so as to give rise to droplet or bubble break-off in the vicinity of an orifice through which both fluids are extruded. Droplets sizes depending on the geometry of channel and flow rate ratio of different fluid phases. Currently, as shown in Figure 24, there are three different gelation techniques commonly used for alginate microgels fabricated on microfluidic chips: (1) internal gelation with calcium carbonate and glucono delta-lactone ($CaCO_3$–GDL) (2) internal gelation with ethylenediaminetetraacetic acid (EDTA)-chelated calcium (CaEDTA–AcOH) and (3) external gelation with $CaCl_2$.[100-102] Advantages and disadvantages are summarized in Table 2. Since we are fabricating functionalized microencapsulated cells as implants, sharp pH change and calcium particle precipitation are not suitable, and thus we choose the method (1) for our design.

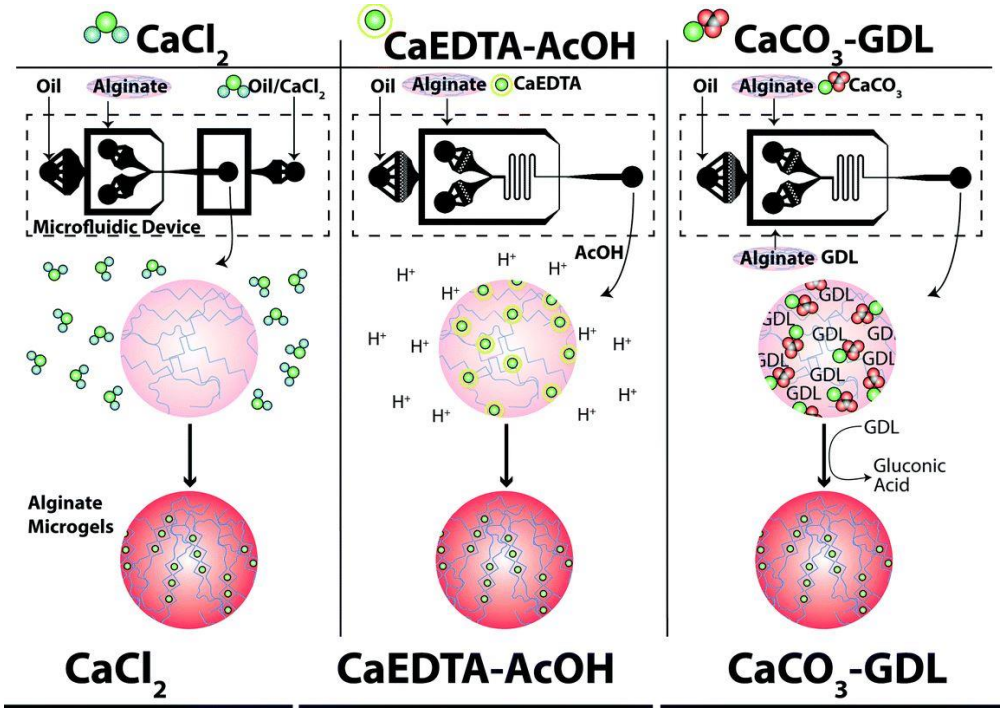

Figure 24. Flow focusing based on-chip gelation methods for alginate particles. Adopted from reference [103].

Methods	Strength	Weakness
Alginate + $CaCl_2$ in oil	Stabilized pH level is good for cells	Low solubility of $CaCl_2$ in oil
Alginate/Ca-EDTA + acidified oil	Internal Ca^{2+} resource and rapid gelation process help shape control	Sharp pH drop can cause cell death
Alginate/$CaCO_3$ + acidified oil	Sufficient internal Ca^{2+} release for gelation without abrupt pH drop	Precipitation of $CaCO_3$ in collected capsules and solutions

Table 2. Pros and cons of three on-chip gelation methods.

To produce microcapsules for parathyroid cells, we adapted a design of a flow-focusing-based 3-inlet multi-layered microfluidic device with two focusing junctions from Dr. Stone research group.[104] Cross-sectional views, with dimensions, of the different sections of the channel are shown in Figure 25. To set up the experiment, the mixture of cells and 1.4% alginate is injected from inlet 1 (inner flow), and calcium iodide in carrier oil is applied in inlet 2 and 3 (middle flow and outer flow, respectively). The oil flow from inlet 2 serves as the cut-off flow to form the small droplet of cells and alginate, and oil flow from inlet 3 helps maintain proper distance between droplets. The alginate droplets can immediately enter the gelation process once they sense the calcium ion in the oil flow and form the microcapsules.

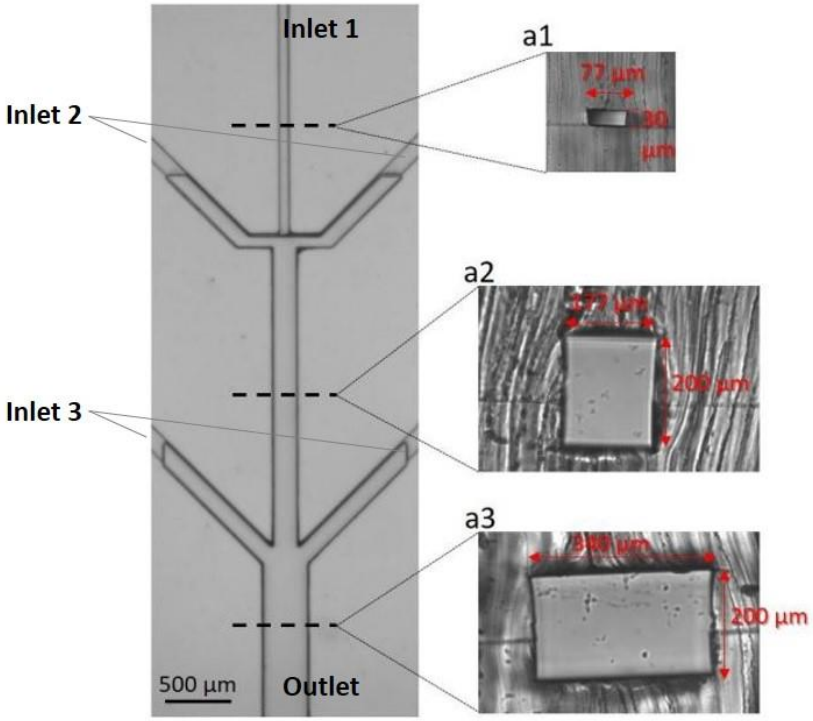

Figure 25. Flow focusing based design of microencapsulator. Design principle was adapted from Howard Stone Research Group in Princeton University. [104]

3.2.2 Device Fabrication

The PDMS device was fabricated using rapid prototyping and soft lithography technique. Details of the protocol were as same as described in 2.2.3.

3.2.3 MIN6 Cell Culture

MIN6 cells in the active phase of growth were cloned by the dilution plating technique. Cells were detached with trypsin in Dulbecco's phosphate buffered saline (DPBS) without Ca^{2+} and Mg^{2+}, and then resuspended in Dulbecco's Modified Eagle Medium (DMEM, 1X) + GlutaMAXTM-I with the addition of 10 % fetal Bovine serum, antibiotics (100 U/ml penicillin and 100 µg/ml streptomycin), 25 mM Hepes, and 285 µM 2-mercaptoethanol. The cell suspension was aspirated gently, with care to avoid separating the cells into a single-cell suspension. Following this, the cells were centrifuged at 1000 rpm for 5 minutes, resuspended in pre-warmed culture medium, counted, and diluted to a concentration of 100 cells/µL in 2mM Krebs-Ringer buffer.

3.2.4 Rat Parathyroid Cell Isolation and Culture

Rat parathyroid glands were identified and removed according to the previously established 5-ALA fluorescent-identification method.[105] In brief, 5-ALA powder (Sigma-Aldrich) was dissolved in 0.5 mL of 0.9% NaCl solution. The 5-ALA solution was then administered (500 mg/kg) by intraperitoneal injection to the rat. After 2 hrs, the rat was anesthetized with compressed CO_2 and 3% isoflurane. A vertical skin incision was made at the midline of the neck, and muscles were dissected until the trachea and thyroid gland were exposed. The fluorescent signal was detected under illumination of a xenon light (380-440 nm) source with an UV filter to locate parathyroid glands. Parathyroid glands were removed by scissor and immersed into PBS in 50-ml tube on ice. After removal of

visible fat tissue, the glands were minced and digested n in 1 mg/ml collagenase P (Roche) in RPMI-1640 media (Sigma-Aldrich) for 30 minutes at 37°C, followed by mechanical disaggregation of shaking and pipetting. Cells were filtered through a 20 µm cell strainer and then centrifuged for 5 min at 800x g. Their viability was then assessed with trypan blue.

3.2.5 Single Cell Microencapsulation

MIN6 cells or isolated rat parathyroid cells were mixed into a 1.4% alginate solution at a cell density of 10^7 cells/mL before the encapsulation experiment. The experiments were set up as described in 3.2.1 and shown in Figure 26, an initial static flow-rate of 50 µL/hr was applied at inlet 1, and the oil phase had a flow-rate of 500-2000 µL/hr at inlet 2 (oleic-acid-based or mineral-oil-based) and a flow-rate of 200 µL/hr at inlet 3. The flow-rate of each fluid stream were adjusted based on the observation to achieve the desired small capsule size of <100 m and high production rate. Capsules were collected in PBS and plated in a small petri dish for imaging under an optical microscope to examine capsule size, morphology, and encapsulation efficiency.

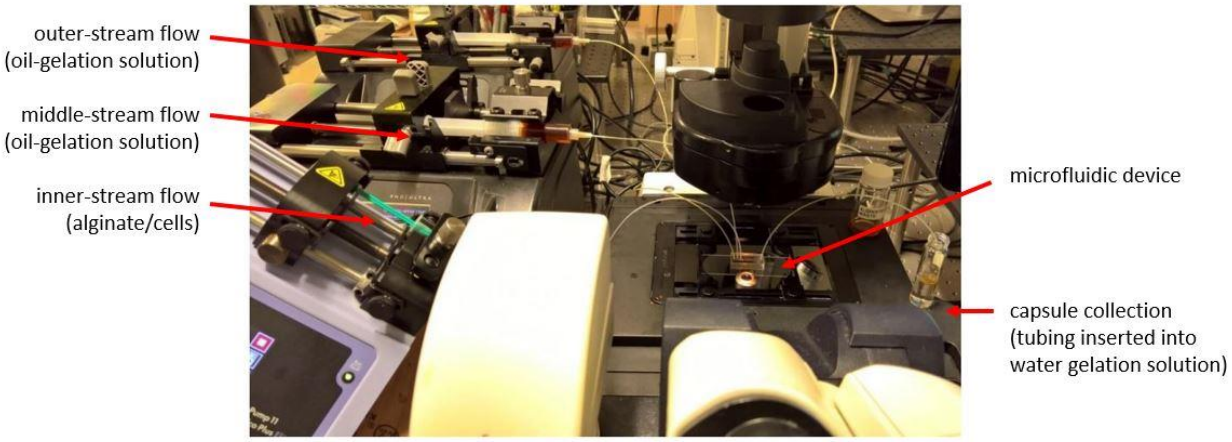

Figure 26. Experimental setup of on-chip microencapsulation.

3.2.6 Viability Test of Microencapsulated Cells

The cell viability in microcapsules will be examined with Fluorescein Diacetate/Propidium Iodide (FDA/PI) fluorescent staining. In brief, FDA and PI were both diluted with 1x PBS solution to achieve final concentrations of 20 µg/mL. Capsules were transferred to the staining working solution with a 100 µL pipette and incubated in the dark at room temperature for 5 minutes. Results of capsule staining were checked under fluorescent microscope. In the blue light excitation of 495 nm, green glow flags living cells, and red flags dead cells, so cell viability can be judged according to the different fluorescence emitted from cells.

3.3 Results and Discussion

3.3.1 Formation of Alginate Beads Using Oleic-acid-based Oil

To determine the proper flow rate range for the generation of micro-capsules, we first investigated the alginate beads formation without cells. For the cell-free tests, we applied 1.4% alginate without cells to the inlet #1 on the device. The production of alginate droplets in the channel was monitored with a high-speed camera, and the alginate beads were collected in a 2-dram glass vial containing approximately 1 mL of the aqueous gelling solution (contains 20 mM Ca^{2+}). The collection vial was then centrifuged at 1000 rpm for 3 min to further transfer the beads to aqueous solution for imaging. We kept the alginate flow at a static flowrate of 50 µL/hr, and the sizes of alginate beads get smaller when the oleic acid oil phase cutting flow had an increasing flowrate from 500 µL/hr to 2000 µL/hr. As shown in Figure 27, the diameter of alginate bead went down to 29.07 µm ± 1.49 which is suitable for single parathyroid cell encapsulation since the size of parathyroid chief cell is around 8 µm.

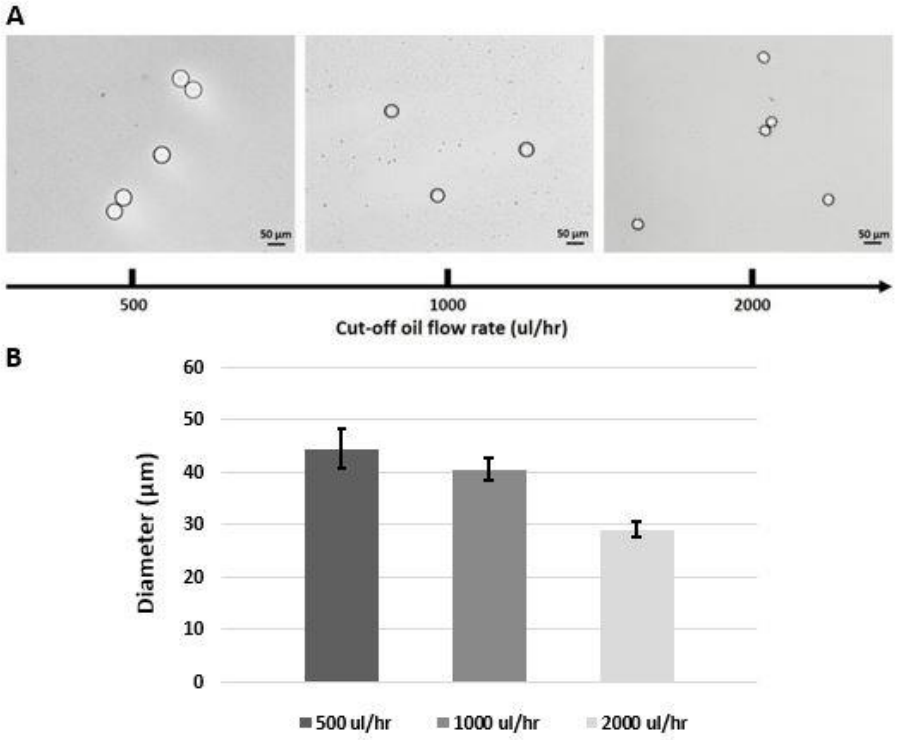

Figure 27. Alginate beads formation using oleic acid served as cut-off oil flow.

The inner flow was maintained at 50 µL/hr, and the outer flow was maintained at 200 µL/hr. A: Images of alginate beads formed at different cut-off oil flow rates of from 500 µL/hr to 2000 µL/hr. B: Diameters of alginate beads formed at different cut-off oil flow rates of from 500 µL/hr to 2000 µL/hr. n=100.

3.3.2 Microencapsulation of Single Cells Using Oleic-acid-based Oil

With the real cell experiments, we used MIN6 cells (mouse pancreatic beta cell line) for the preliminary tests. By mixing the cells suspension in PBS buffer without calcium with 1.5% alginate solution, we reached the final concentration of alginate at 1.4% and applied this cell/alginate solution for inlet #1 on the device. The results are shown in Figure 28. With the static flow rate of 50 µL/hr, the sizes of microcapsules were getting smaller down to 67.42 µm ± 2.54 when the oleic acid oil phase cutting flow had an increasing flowrate from 500 µL/hr to 2000 µL/hr. This result shows that microcapsules with cells are bigger than the pure alginate beads at the same condition of flow dynamics. The different sizes can be explained due to the density change from adding cells, but the size of microcapsules we produced is still in the good range (<100 µm) which is much smaller than the ones (500-1000 µm) in previous studies of implantable microcapsules.

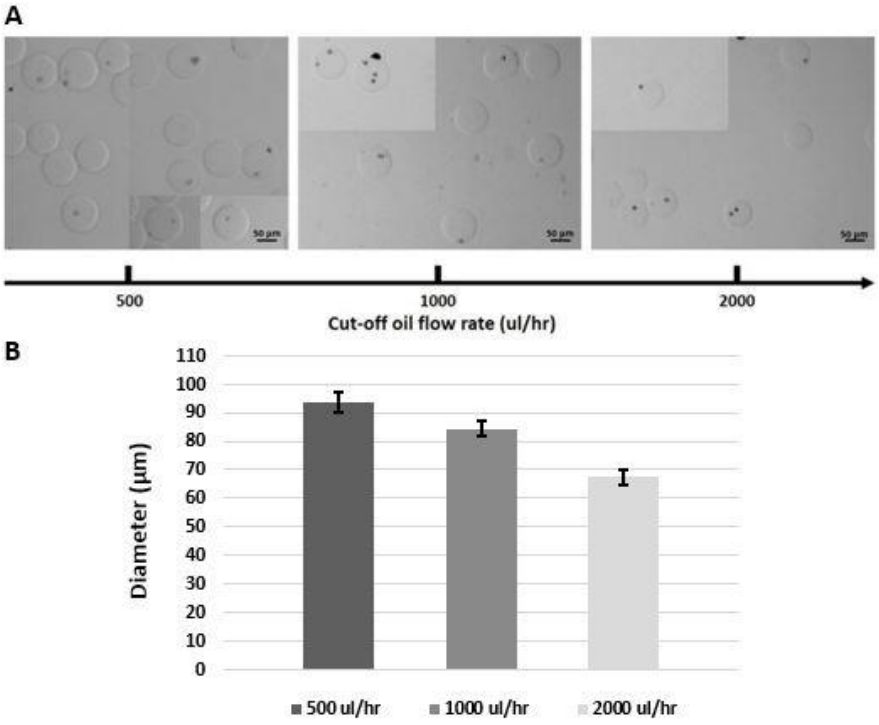

Figure 28. Microencapsulation of MIN6 cells using oleic acid served as cut-off oil flow. The inner flow was maintained at 50 µL/hr, and the outer flow was maintained at 200 µL/hr. A: Images of alginate beads formed at different cut-off oil flow rates of from 500 µL/hr to 2000 µL/hr. B: Diameters of alginate beads formed at different cut-off oil flow rates of from 500 µL/hr to 2000 µL/hr. n=100.

Since the oil-phase cut-off flow dominates the overall flow rate in the main channel, we optimized the production frequency of microcapsules by changing the cut-off oil flow. As shown in Figure 29, higher flow rate would cause higher production rate up to ~1800 capsules/min at cut-off flow rate of 2000 µL/hr. The production frequency, theoretically, can be further increased with higher flow rate in the channel, but it would cause problems, such as in-channel pressure accumulation and incomplete gelation of microcapsules. The geometry needs to be lightly modified to expand the channel if there is a need to fabricate a high volume of microencapsulated cells, for example, transplant to human patients.

Beside the production rate, the encapsulation efficiency is also crucial to evaluate a microencapsulation method. In our previous study with islet encapsulation, ~50% of capsules were empty and manually removed in the final washing step before culture. With the new microfluidic design and cell density of 10^7 cells/mL in preparation of alginate/cell suspension, we were able to consistently generate the efficiency of above 80%. Ideally, the efficiency can be further increased and close to 100% when we have extremely high cell density in the preparation of cell suspension with alginate. But in that case, the large cell numbers in random capsules will be hard to handle and may leading to the destruction of capsule structures. Also, the alginate concentration can be dramatically affected when there are too many cells in the suspension solution.

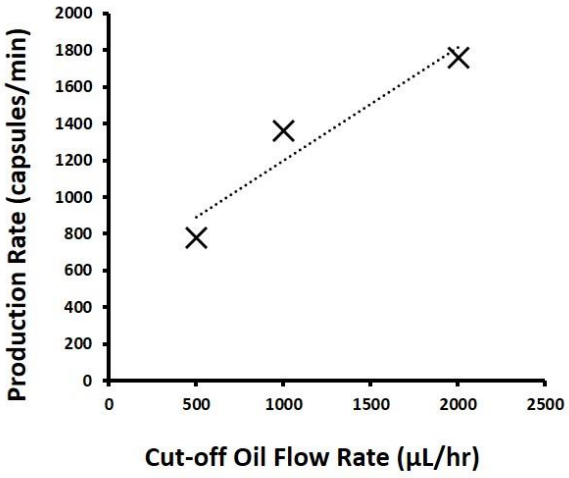

Figure 29. Frequency of cell microencapsulation on-chip.

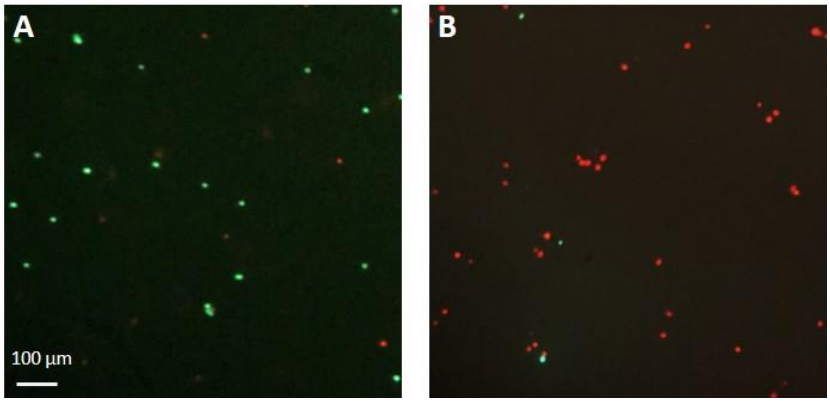

Figure 30. Viability of microcapsules fabricated using oleic acid as calcium carrier oil flow. FDA/PI staining was applied to reveal the cell viability. Green color indicates alive cells and red color indicates dead cells. A: Control. B: Collected microencapsulated MIN6 cells with oleic acid based setup.

Viability tests were performed with microencapsulated MIN6 cells and results are shown in Figure 30. A poor viability (~10% alive) was observed in the collected microencapsulated cells compared to the control (>90% alive). We further tested the toxicity of all the materials we used separately on-bench in the MIN6 cell culture and found the cell death caused by the cytotoxicity of oleic acid. With some literature review, we realized that oleic acid can promote apoptosis and necrosis of cells. The mechanism of cell death induced by these fatty acids seem to involve with mitochondrial depolarization, lipid accumulation and the levels of C-MYC and P53 mRNA expression.[106] In our experimental setup, we were using oleic acid as the carrier flow for calcium ions and that would provide a harmful environment of high concentration oleic acid, which would lead to cell death immediately. So, we had to move on and tried to find another oil phase carrier for calcium-mediated gelation.

3.3.3 A Possible Answer – Mineral-oil-based Oil

As previously reported, the light mineral oil was applied as the oil phase flow for droplet formation and cell microencapsulation in microfluidic channels due to its non-toxicity and accessibility.[107] Unlike calcified oleic acid, calcium cannot dissolve in mineral oil. Surfactants are chemical compounds, which are able to lower the surface tension in between two liquids or between a liquid and a solid. With the help of a surfactant, Span 80 often applied, and after sonicating mix, extremely small $CaCl_2$ aqueous drops can form and suspend in mineral oil for a few hrs. So, mineral oil can serve as a carrier of calcium in our design for cell microencapsulation.

Similar to the experimental setup with oleic acid previously described, the mixture of cells and 1.4% alginate is injected from main channel, and calcium chloride in mineral

oil is applied as cut-off flow and space-maintaining flow. Particularly, to prepare calcium in mineral oil, a 1: 9 volumetric mixture of 0.7 g/mL $CaCl_2$ and light mineral oil with 1.2% Span 80 (Sigma) was sonicated for 20 minutes before use. From our experience, the aqueous phase started separating from oil phase after 1-2 hrs and thus the mixture solution would need to be sonicated every 1-2 hrs.

Once again, we tested the alginate formation in the new experimental setup with mineral oil and images are shown in Figure 31A. Overall, the gelation of alginate microbeads went smoothly, but was not completed. Alginate beads showed a wider size range than those collected from oleic acid experiments, with an average diameter of 46.36 μm ± 9.01. The size and shape variations were resulted from incomplete gelation of alginate. The reason of this can be explained as that the effective calcium concentration, which is the concentration of calcium contacted with alginate and got involved in its gelation process, is lower in mineral oil flow than calcified oleic acid flow, since $CaCl_2$ is not dissolvable in mineral oil but can be dissolved in oleic acid. Furthermore, we used MIN6 cells for tests of microencapsulation of single cells and results are shown in Figure 31B. As observed previously in the formation of alginate beads, the microcapsules were not perfectly circular due to the incomplete gelation. However, cells were efficiently microencapsulated in alginate, with an average diameter of 57.14 μm ± 5.35.

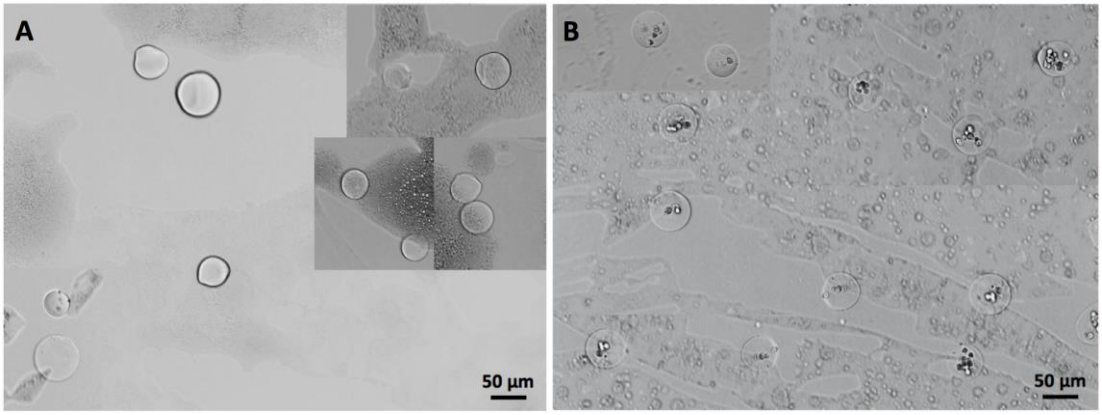

Figure 31. Alginate microcapsule formation without and with cells using mineral oil based experimental setup. A: The inner flow was maintained at 50 µL/hr, and the outer flow was maintained at 200 µL/hr. A maximum flow rate of 1500 µL/hr was applied for cut-off oil flow to fabricate the minimize the capsule size. B: With MIN6 cells incorporated.

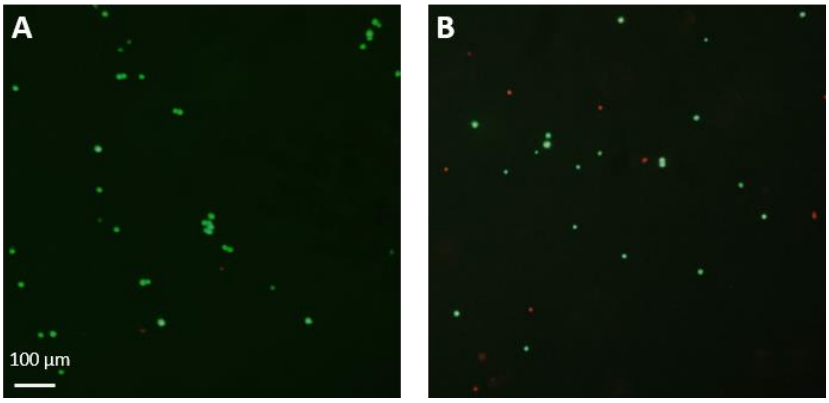

Figure 32. Viability of microcapsules fabricated using oleic acid as calcium carrier oil flow. FDA/PI staining was applied to reveal the cell viability. Green color indicates alive cells and red color indicates dead cells. A: Control. B: Collected microencapsulated MIN6 cells with mineral oil based setup.

We performed viability tests to microencapsulated cells by using FDA/PI staining. As shown in Figure 32, compared to the control group with ~90% viable cells, the viability of microencapsulated cells from the new mineral-oil-based method remained ~70%, which is a big improvement from what we obtained from oleic-acid-based experiments. This result gave us a positive signal that mineral oil can be a possible answer to our current issue of cell viability, and may provide the chance to move on to next stage of this project when we solve the remaining issue of incomplete gelation of alginate particle.

3.3.4 Isolation and Microencapsulation of Rat Parathyroid Cells

Surgical excision of rat parathyroid glands was performed following a protocol of hypoparathyroidism rat animal model established previously.[108] As shown in Figure 33, the fluorescent-identification method allowed us to easily locate the glands under the ultraviolet light followed by intraperitoneal 5-ALA injection. Glands collected were enzymatically digested and filtered to obtain the parathyroid cells. The viability of cells was 70% and dropped down to 40% after overnight incubation. There can be many contributors to the cell loss and death, such as unskilled surgical operation, enzymatic over-digestion, temperature control, animal health issues and so on. The protocol is still under optimization and needs to be improved in the future work.

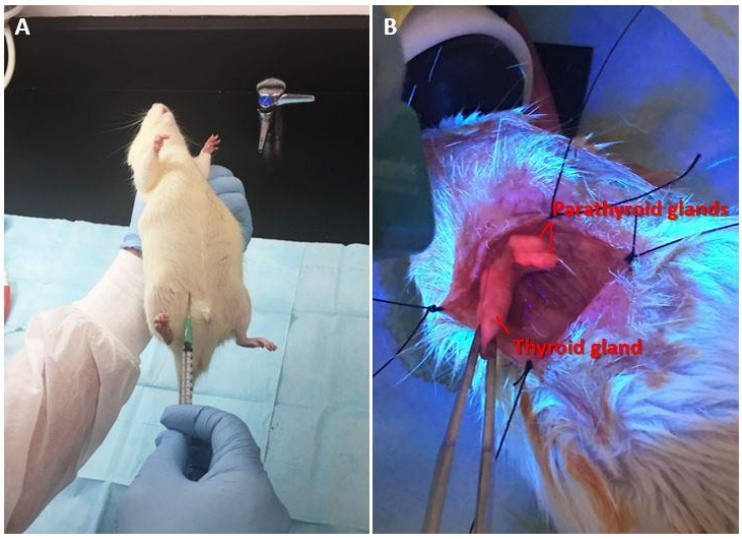

Figure 33. ALA-5 mediated fluorescent-identification of rat parathyroid glands. A: Intraperitoneal injection of ALA-5 to rat. B: Identification of rat parathyroid glands under an ultraviolet light source.

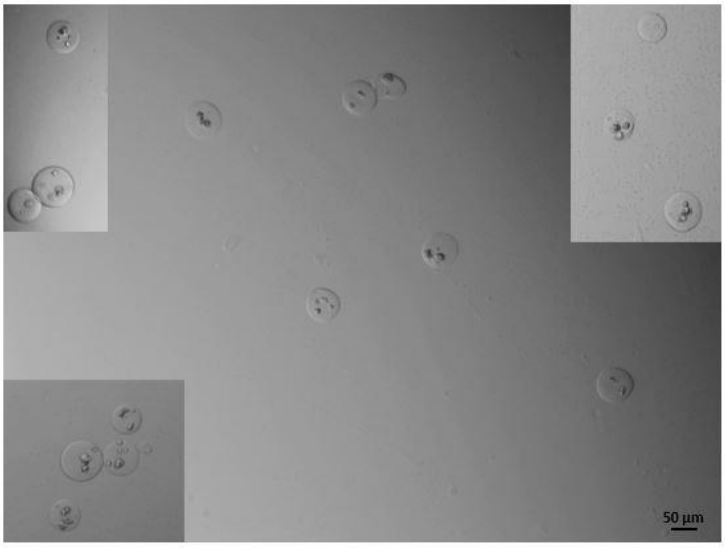

Figure 34. Images of microencapsulated rat parathyroid cells. The inner flow was maintained at 50 µL/hr, and the outer flow was maintained at 200 µL/hr. A maximum flow rate of 1500 µL/hr was applied for cut-off oil flow to fabricate the minimize the size of parathyroid cell microencapsules.

To test the device, we microencapsulated rat parathyroid cells from isolation, and images of capsules are shown in Figure 34. Although the viability was low due to cell isolation issues, we still could fabricate parathyroid cell microcapsules with average diameter of 66.67 μm ± 6.65, which had similar size ranges and circular shapes with previous microencapsulation of MIN6 cells. This further confirmed that we were ready to move on this project to cell functional examinations once we have more optimized protocol of parathyroid cell isolation to reach a higher viability.

3.4 Conclusion and Future Direction

3.4.1 Conclusion

In this project, we developed a novel microfluidic platform for parathyroid cell microencapsulation in which microcapsule formation and capsule gelation are performed in subsequence within a single device. Different flow-rates in microfluidic channels and multiple gelation parameters (alginate concentration, calcium concentrations in oil/aqua gelation solution, cell loading density) were investigated to study the gelation process. With this flow-focusing-based microencapsulator device, we can achieve a high production rate and efficiency of microcapsules formation, which has been shown difficult to achieve in traditional cell encapsulation methods. The high viability of encapsulated cells was also achieved when we switched to mineral-oil-based oil phase flow as the calcium carrier. To acquire the consistent shape of individual capsules, either the elongated channel design or modified collection methods can be helpful to improve the gelation process.

3.4.2 Next Step – *In Vitro* and *In Vivo* Functional Tests

Despite the minimal variation of shape and size of microcapsules, cells can remain viable during the microencapsulation process with mineral-oil-based setup and ready to move on to *in vitro* and *in vivo* functional tests.

Physiologically, the relation between PTH secretion and extracellular calcium concentration is defined by a sigmoid curve. Thus, the reduction in calcium concentration produces an increase in PTH secretion until it reaches a maximum; an increase in calcium concentration, in contrast, reduces PTH secretion to a minimum. The *in vitro* functional test aims to confirm this stimulation of microencapsulated parathyroid cells by calcium solutions of different concentration. Following a protocol established previously, the microencapsulated parathyroid cells will be sequentially transferred at 1 hr intervals to different wells of a multi-well plate containing solutions with variable concentrations of calcium: 0.4, 0.6, 0.8, 1.0, 1.25, and 1.35 or 1.5 mM.[109] PTH secreted from parathyroid cells will be examined by ELISA. The results from previous study and also expected from our *in vitro* test are shown in Figure 35.

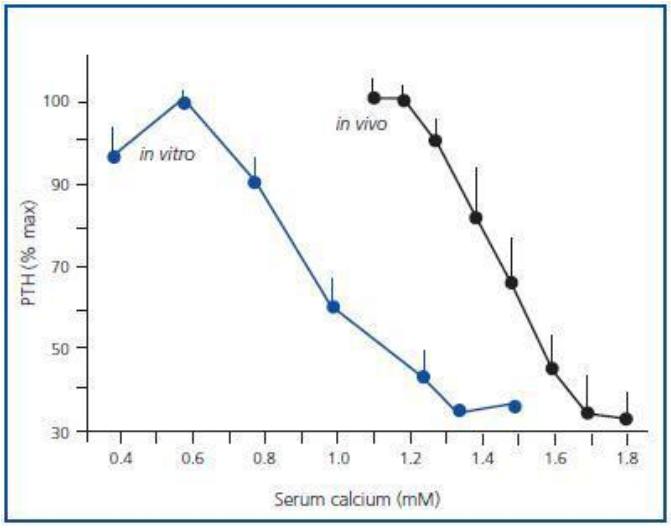

Figure 35. Previous in vitro and in vivo studies of rat blood serum PTH level in responding to varied serum calcium concentration. Adopted from reference [109].

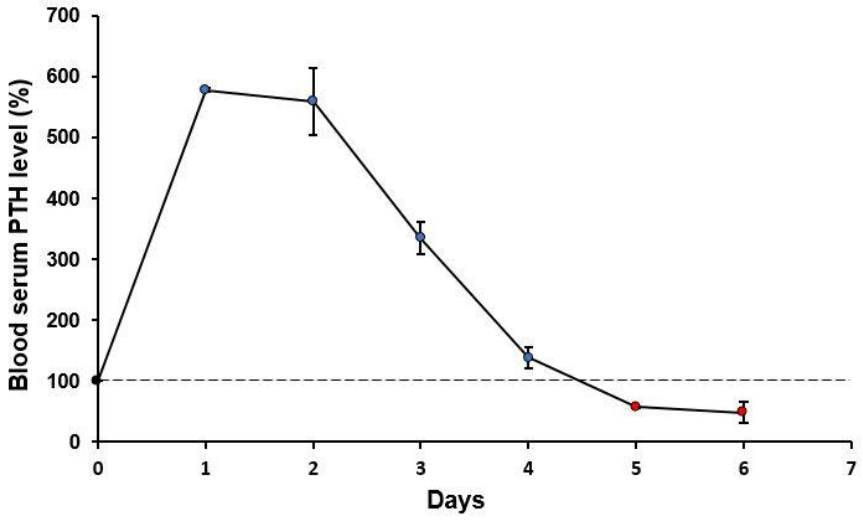

Figure 36. Post-surgical blood PTH measurement of parathyroidectomized rat. PTH in blood serum samples collected over a week following the parathyroidectomy surgery were measured with ELISA and normalized to percentage.

For *in vivo* tests, we are planning to use the rat hypoparathyroidism model created by excision of parathyroid glands following the protocol described above in the 3.2.4. After surgery, blood PTH level will be monitored over a week to confirm the hypoparathyroidism condition. A preliminary test showed a decrease of blood PTH starting from 3rd postoperative day as shown in Figure 36. The blood PTH dropped to below per-surgical level at day 5, but remained in detectable range. This could be result from incomplete excision of parathyroid glands. At day 7, the rat died probably due to infections. Ideally, parathyroid cell microcapsules will be injected into the peritoneal cavity through a tubing connected to a syringe based on our previous experience with encapsulated pancreatic islets transplantation.[110] As a result, the hypoparathyroidism condition of rat is expected to be reversed and will be confirmed by monitoring blood PTH and calcium level over weeks.

In summary, we are capable of efficiently fabricating microencapsulated parathyroid cell with our microfluidic microencapsulator device. Our new mineral-oil-based setup provides a non-toxic environment to maintain the high viability of cells during microencapsulation process, although size and shape variation of microcapsules caused by incomplete gelation will require further configuration. The microencapsulated parathyroid cells are potentially surviving and functioning for a relatively long term after transplantation due to the protection of hydrogel layer and can be a possible alternative treatment to hypoparathyroidism.

4. A NOVEL SINGLE CELL LEVEL MICROFLUIDIC PERFUSION SYSTEM

4.1 Introduction

4.1.1 Stem Cell-based Therapy Development

Globally, many researchers are evaluating the potential of stem cells as protagonists for clinical applications, including drug screening, regenerative medicine and modeling of disease development. In the translational study, there are many stem cell types holding huge potential to develop novel cellular products. The commonly used stem cells include human pluripotent stem cells (hPSCs), comprising human embryonic stem cells (hESCs) and induced pluripotent stem cells (iPSCs), hematopoietic stem cells (HSCs), mesenchymal stem/stromal cells (MSCs), and tissue-specific stem cells from various tissue sources.[111-114]

In the development of a new stem cell based therapy, it is vital to control cellular microenvironment to study cellular phenotype for purposes of either toxicity screening or tissue repair. In terms of translation to the clinic application, in which extremely large number of cells would be needed for each transplant, an improved protocol with enlarged scale bioprocessing will require finer microenvironmental control of stem compared to standard scale protocol. In addition, the quality, efficacy, and safety of the stem cell derived product must have strict control and assurance.[12] To address all these issues and maintain a high-performance bioprocess is crucial to support the development of stem cell therapy.

4.1.2 Dynamic Single Cell Analysis

Researches in stem cell biology and biomedical science mostly rely on how cells behave in different conditions and respond to different stimulation.[115] Fate of stem cells is closely related to their exocellular microenvironment, which can affect cell differentiation and proliferation, because cell-cell communications and cell-extracellular matrix (ECM) contacts usually play key roles in cell signaling pathways.[116] Also, physically, mechanical factors, like shear force, can contribute a lot to cell maturation and characterization.[111, 117-123] Unrevealed signaling pathways and mechanisms lead to stochastic behavior in cell behaviors. The heterogeneity showed on the analysis of individual single cells can be used to study the distribution in cell responses and further discover the mystery of life.[124-126] Recently, researchers attempt to build *in vitro* analytical systems with high efficiency and resolution for single cells study that allows dynamic analysis of biomolecules or signals involved in cell behaviors in changing microenvironment.

4.1.3 Perfusion-based Microfluidic Platform for Single Cell Analysis

Cell perfusion is a method to study the cell behavior in a dynamic environment, in which it uses fluid flow as the carrier of multiple physical or chemical parameters to stimulate the cells and collect subsequent information, often applied in studies of stem cell differentiation, screening and characterization for stem cell therapy development (Figure 37). Since a microfluidic system has the ability to control the fluid at a volume scale of microliters to mimic the cellular microenvironment, a high-throughput study of biological pathways at single cell level is enabled on this platform. For example, microfluidic systems can be applied to manage the extracellular microenvironment to

study cell phenotype and behavior. Moreover, as previously reported, shear stress showed impacts on cell growth and differentiation, so with the precise control of fluid flow in micro-channels, the shear affects can be explored.[127]

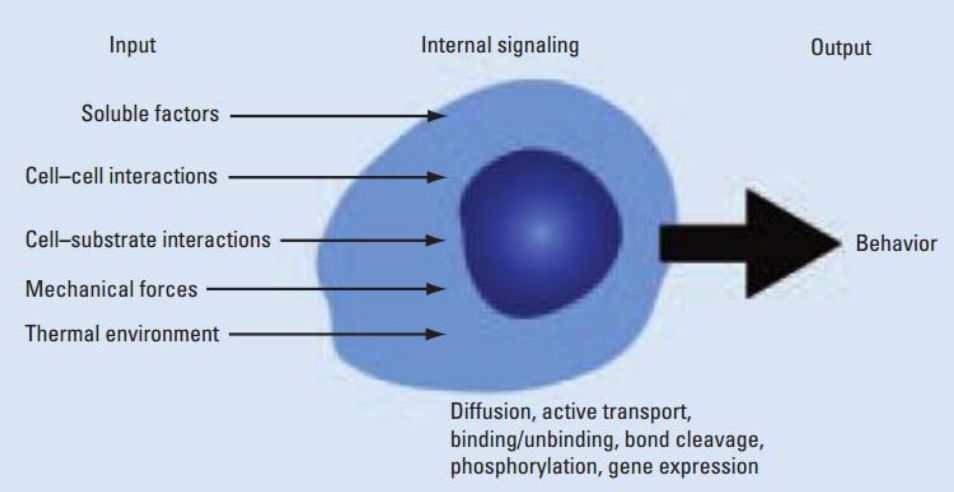

Figure 37. Input-output response for the cellular machine. Adopted from reference [115].

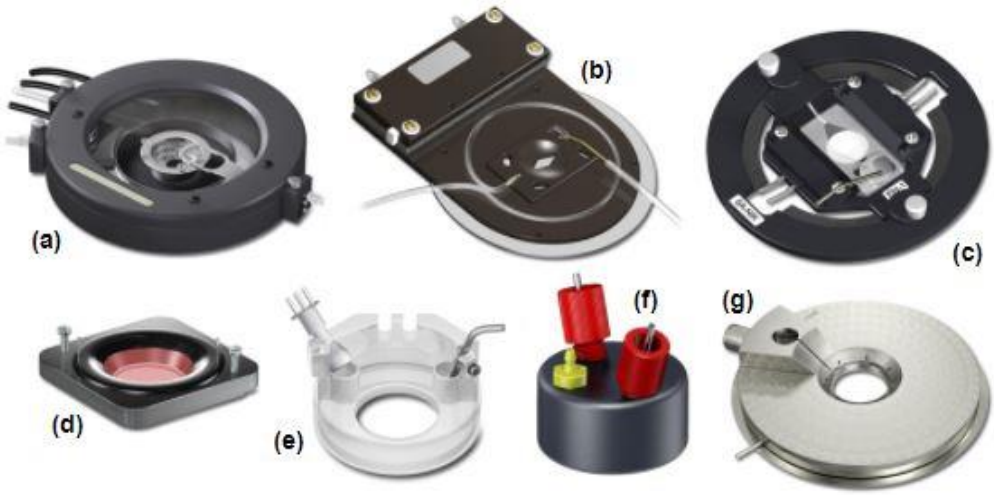

Figure 38. Commercial live-cell perfusion chambers. (a) is a self-contained environmental chamber that houses a Petri dish along with capabilities for perfusion. (b) depicts a diamond-shaped perfusion chamber in a heated stage adapter. (c) illustrates a similar design, but with a circular chamber. (d) is a Ludin-style perfusion chamber capable of being mounted in a rack. (e) is a Petri-style perfusion chamber molded to contain ports for introduction and exhaust of perfusion fluids. (f) contains ports and is designed to insert into standard 6-well plates that contain adherent cells on the plastic growth surface. (g) is designed to be mounted on a microscope stage with a circular aperture, and is provided with several ports around the perimeter of the central well. Adopted from https://www.microscopyu.com/applications/live-cell-imaging/live-cell-imaging-culture-chambers.

In order to completely apply the advantages of microfluidic integrated cell perfusion assays, methods for long-term cell immobilization at defined locations are vital. Figure 37 shows the current perfusion chamber for cell dynamic imaging commercially available and it requires an extra step of cell pre-culture allowing cell attachment on chamber surface before the perfusion experiment. Microfluidic technique has showed strength in manipulation of fluid flow in microchannel and thus provides opportunities of cell immobilization without cell attachment. Specifically designed micro-scale features allow the cell immobilization even for non-adherent cells, which is especially useful for analysis of cells derived from stem-cell. For example, micro-sized wells were integrated in our previous design of perfusion chamber to immobilize pancreatic islets, as shown in Figure 39A.[57] In addition, researchers have also developed many microfluidic cell trapping systems for cell analysis at single cell level (some examples are shown in Figure 39B-D).[57, 128-130] However, the fabrication difficulty and low trapping capacity are limitations for the applications of cell-based therapy development and may cause issues such as complicated experimental operation and insufficient sample collection and measurement of cellular secretion. Therefore, an easy-use, reusable and efficient perfusion system with microfluidic techniques can be a powerful tool in the development of cell-based therapy.

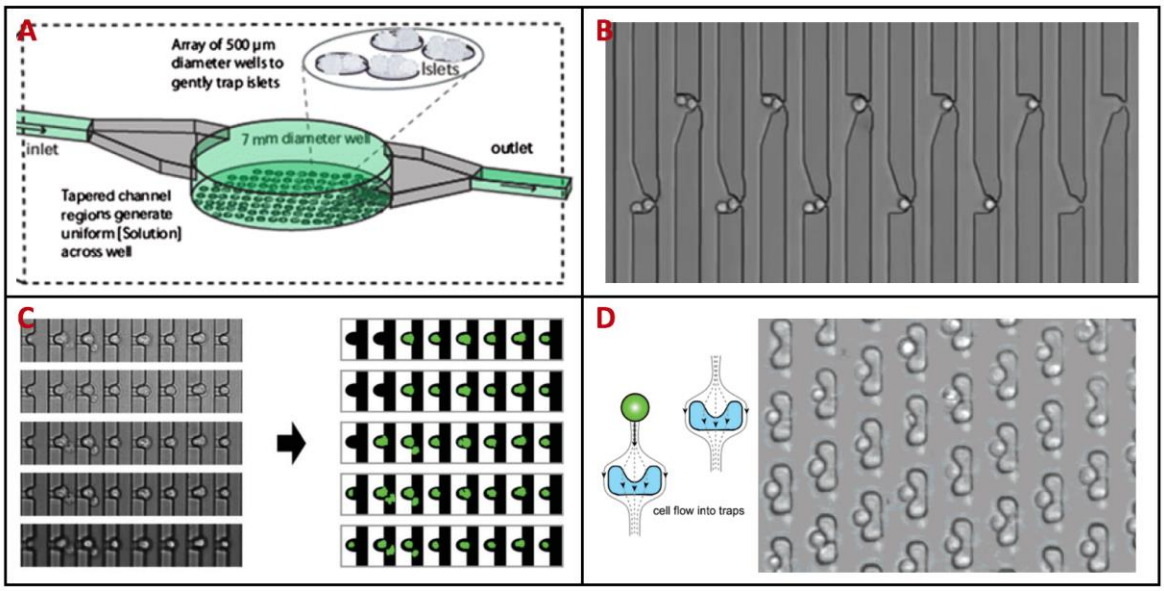

Figure 39. Examples of cell immobilization in microfluidic design. A: Microwells structure for trapping pancreatic islets in our previous design of islet perifusion chamber. Adopted from reference [57]. B: Hydrodynamic trapping of single stem cells. Adopted from reference [130]. C: Another design of single cell trapping array based on hydrodynamic trapping principle for RNA analysis. Adopted from reference [129]. D: An array of individual traps for single-cell enzyme concentrations, kinetics, and inhibition analysis. Adopted from reference [128].

4.2 Materials and Methods

4.2.1 Device Design of Single Cell Level Perfusion Chamber

As shown in Figure 40, the new perfusion chamber device we designed has two trapping structures, sample windows fulfilled with small trapping wells of 60 μm diameter on the surface for the single cell imaging, and a reusable 0.22 μm filter membrane for mass cell trapping and perfusion. To set up the perfusion experiment, we first slowly load the cell suspension through the loading port of the device fulfilled with buffer solution and wait for them settling down to the trapping areas, and then block the loading port. During the perfusion, different solutions can be switched to the inlet port, and cell secretion is collected from the outlet port for later measurement.

4.2.2 Computational Flow Simulation

Two-dimension (2D) computational fluid dynamics (CFD) simulations were performed in COMSOL Multiphysics 5.0 (COMSOL, MA) using a ‘stationary laminar flow’ model. The pressure from surface tension of a 10-μL droplet was applied as the initial inlet pressure, and both the backward pressure and gravitational force were ignored as discussed previously. No-slip boundary conditions were applied to the walls of the channels. The complete mesh consisted of 60,478 domain elements and 4,033 boundary elements. Error tolerance was 10^{-6}.

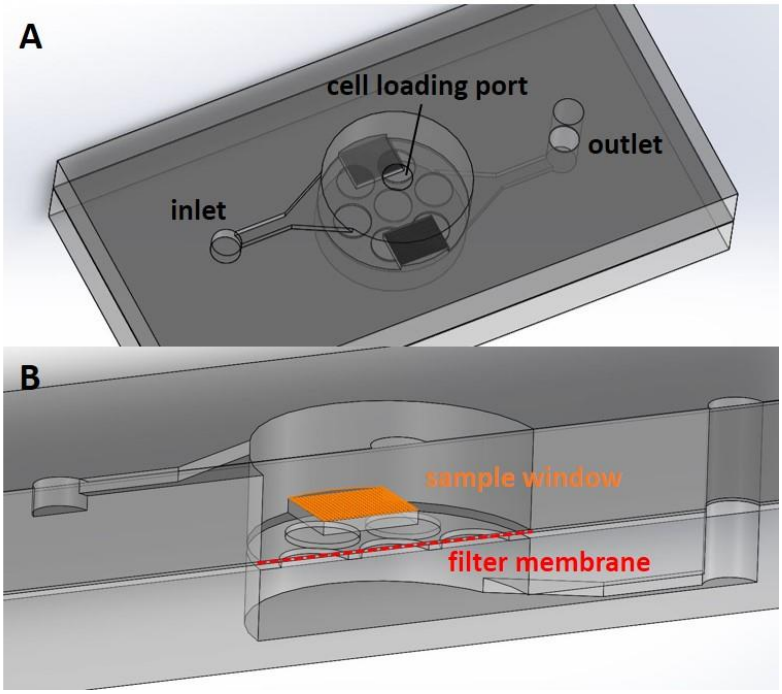

Figure 40. The design of dual-chamber perfusion system. A: A schematic of perfusion chamber device. B: Cross-section of the chamber. The “sample window” is the area designed to trap individual cells in multi-microwell structure, while the filter membrane with 0.22 µm pores is applied for massive trapping of the rest of loading cells.

4.2.3 Device Fabrication

The PDMS device was fabricated using rapid prototyping and soft lithography technique. Details of the protocol were the same as those described in the 2.2.3.

4.2.4 Islet Cell Dissociation

Islets were rinsed three times by Dulbecco's phosphate-buffered saline (DPBS) without Ca^{2+} and Mg^{2+} and centrifuge at 1000 rpm for 5 min. The trypsin-EDTA solution (Sigma-Aldrich) was applied and incubated with cells at 37°C for 10 min. After FBS neutralization, pipette the cell suspension up and down with a 200ul pipet tip until a single cell preparation was obtained. Single cells were filtered with 35-micron filter (Fisher Scientific) and collected in a culture dish with culture medium. Islets dissociated by this method provided a predominantly (80-95%) single cell preparation of 2000-2500 cells per islet. Cell viability was > 90%.

4.2.5 Perfusion and Fluorescence Imaging of Islet Single Cells

In brief, the islets were incubated in 2 mL of Krebs buffer containing both 5 µM Fura-2/AM and 2.5 µM Rhodamine 123 fluorescent dyes (Molecular Probes, CA) for 30 minutes prior to loading to the device. The islets were then loaded into the temperature equilibrated microfluidic device mounted on an inverted epifluorescence microscope (Leica DMI 4000B). Dual-wavelength Fura-2/AM was excited at 340 and 380 nm and fluorescent emission was detected at 510 nm. Intracellular Ca^{2+} was expressed as a ratio of fluorescent emission intensity F340 / F380 (%). Rh123 was excited at 490 ± 10 nm, and emission was measured at 530 ± 10 nm. Fura-2 and Rh123 fluorescence emission spectra were filtered using a Fura-2/FITC polychroic beamsplitter and double band emission filter (Chroma Technology). These images were collected with a CCD (Retiga-

SRV, Fast 1394, QImaging). SimplePCI software (Hamamatsu Corp) was used for image acquisition and analysis. Both fluorescence signals were expressed as “change-in-percentage” after being normalized against basal intensity levels established before stimulation.

4.2.6 Insulin Collection and ELISA

Insulin concentrations were measured using Mouse Insulin ELISA kits (Mercodia AB, Uppsala, Sweden) according to provided protocols using Biotek Synergy 2 microplate reader (BioTek U.S., Winooski, VT).

4.3 Results and Discussion

4.3.1 Flow Dynamics in Perfusion Chambers

The computational simulation was done with COMSOL Multiphysics. The cross-section view of the flow simulations of the old and new design of perfusion chamber are shown in Figure 41, and the comparison indicates that in the new design, there is an efficient perfusion without any dead corners of the flow, which will affect the detection resolution and sensitivity of secretion measurement based on our previous observation in the old design.

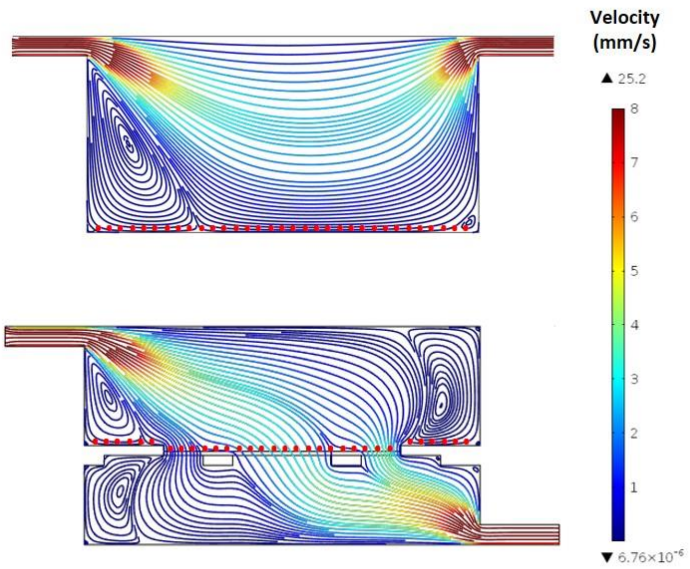

Figure 41. Flow dynamic simulation of both our previous perfusion chamber device (top) and new design (bottom).

4.3.2 Fluorescence Imaging of Rodent Islet Single Cells

C57B6 mice were used to isolate pancreatic islets following the established protocol from previous study. Dissociated islet single cells, which has beta cells as the majority of cell population, were cultured with fura-2 as the indicator of intracellular calcium level and then loaded carefully through the loading port on the device. During the perfusion test, real-time fluorescent imaging was analyzed with computer and secreted insulin samples were collected over time. As a comparison, our previous perfusion chamber device was also used to run the tests. In Figure 42, the typical stimulation curve from the new design can be observed where the $[Ca^{2+}]_i$ of islet beta cells increased up to ~135% in response to 14 mM glucose and ~145% in response to 30 mM KCl. The similarity on the profiles of stimulation curves between the new and old perfusion chamber devices showed that the fluid delivery was efficient enough for cell stimulation assays.

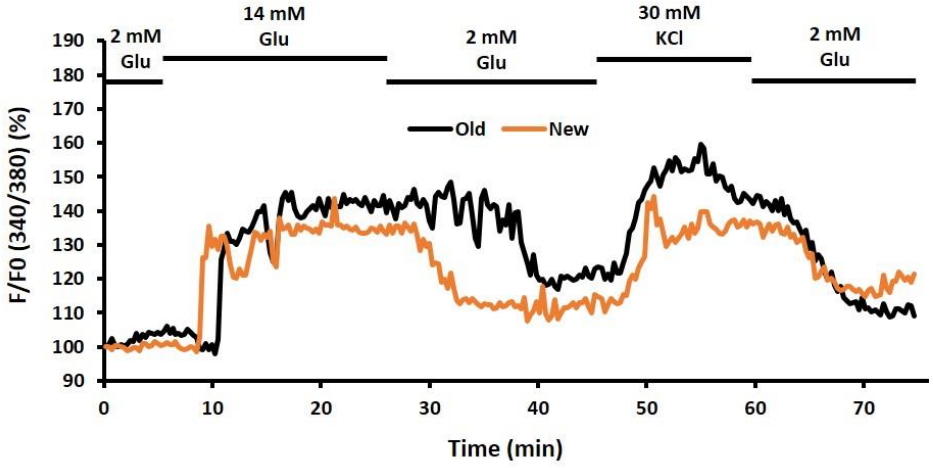

Figure 42. Representative trace of rodent islet calcium signaling in response to 14 mM glucose and 30 mM KCl from perfusion experiments of both old and new design of perfusion chambers. N = 50 - 60 islets from three independent islet samples.

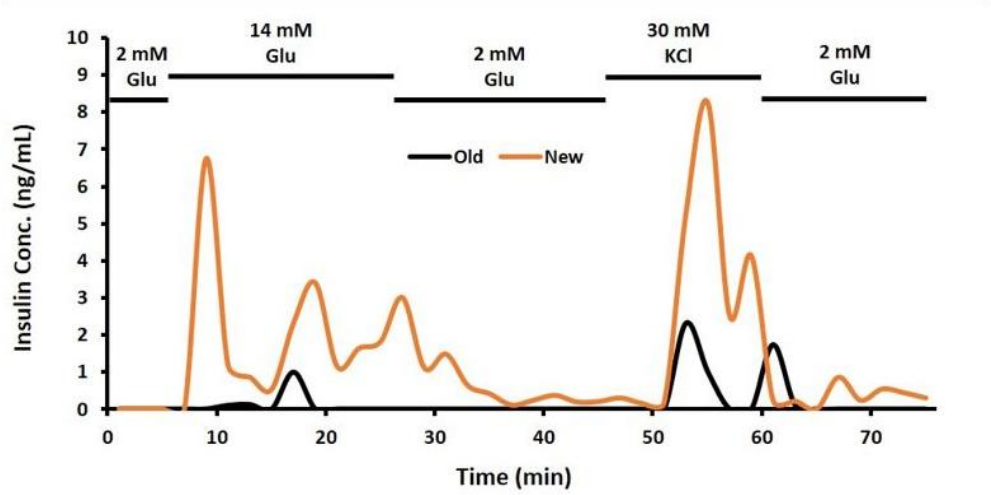

Figure 43. Representative trace of rodent islet insulin secretion in response to 14 mM glucose and 30 mM KCl from perfusion experiments of both old and new design of perfusion chambers. N = 3 in ELISA measurements.

4.3.3 Insulin Secretion of Rodent Islet Single Cells

In Figure 43, the result from rodent insulin ELISA showed a typical profile with a peak concentration of 6.75 ng/mL in response to 14 mM glucose and another peak concentration of 8.25 ng/mL in response to 30 mM KCl from the sample collection from the new perfusion chamber device, but not obviously from the old one. This is a good demonstration that our new perfusion chamber device can be a promising tool for single cell level studies.

4.4 Conclusion and Future Works

4.4.1 Conclusion

In conclusion, we developed a new microfluidic perfusion system for single cell analysis. In contrast to previous perfusion-based chamber device, our new design provides an opportunity for both single cell fluorescent imaging and, simultaneously, cell secretion collection of massive loaded single cells due to the features of single and massive cell-trapping areas. This is meaningful in cell physiological study, cellular factor screening, and cell characterization involved in the development of stem cell therapy.

4.4.2 The Future: A Perfusion Chamber for Both Single Cells and Cell Clusters

To further improve the design, we can consider about the possibility of combining the perfusion functions of both single cells and cell clusters in one chamber. In another word, microwells on trapping windows for cell imaging can be varied on size to trap from single cells to cell clusters. The concept of this perfusion chamber is shown in Figure 44. This design can be beneficial not only because it provides cell trapper on varied sizes which can fit different cases without fabricating specific device, but it also very useful in particular cases. For example, based on our previous experience, stem-cell-derived cells

can behave differently from separated single cells to cell aggregates, and even if the function units have to be cell clusters, the cell function can be cluster-size-related. To better understand the physiological reasons of cell behaviors, such a perfusion chamber with capability of examine both single cells and cell clusters would be a helpful contributor to the development of cell-based therapy.

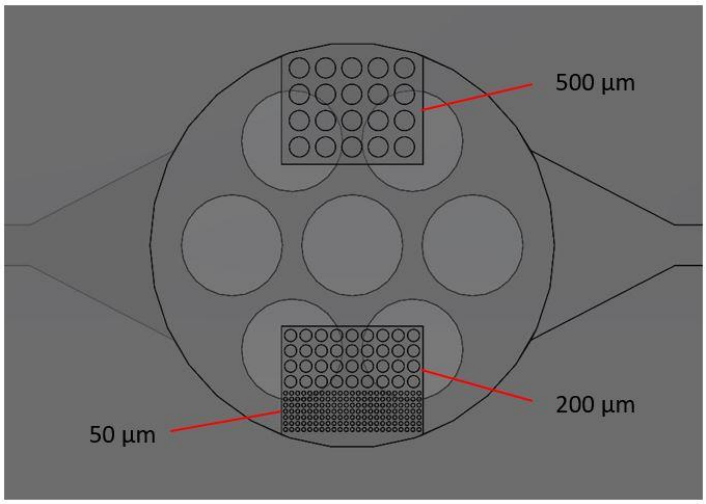

Figure 44. Future direction of design with varied-sized microwells on sample trapping windows. Microwells of three different sizes (diameters of 50 µm, 200 µm and 500 µm) are applied as examples in this design, however, more options on size can be added based on needs.

APPENDIX

Permission to re-use author's previously published article in this dissertation.

SPRINGER LICENSE
TERMS AND CONDITIONS

Jul 25, 2017

This Agreement between Yuan Xing ("You") and Springer ("Springer") consists of your license details and the terms and conditions provided by Springer and Copyright Clearance Center.

License Number	4155990788446
License date	Jul 25, 2017
Licensed Content Publisher	Springer
Licensed Content Publication	Biomedical Microdevices
Licensed Content Title	A pumpless microfluidic device driven by surface tension for pancreatic islet analysis
Licensed Content Author	Yuan Xing
Licensed Content Date	Jan 1, 2016
Licensed Content Volume	18
Licensed Content Issue	5
Type of Use	Thesis/Dissertation
Portion	Full text
Number of copies	1
Author of this Springer article	Yes and you are the sole author of the new work
Order reference number	
Title of your thesis / dissertation	Microfluidic Platform for In Vitro Study on the Development of Cell Therapy
Expected completion date	Nov 2017

REFERENCES

1. Lefrere, J.J. and P. Berche, *[Doctor Brown-Sequard's therapy].* Ann Endocrinol (Paris), 2010. **71**(2): p. 69-75.
2. Niehans, P., *[20 Years of cellular therapy].* Med Klin, 1952. **47**: p. 1-16.
3. Pagano, L. and S. Lyon, *Celebrating 40 years of progress in bone marrow transplantation: a report from the 40th Annual Meeting of the European Society for Blood and Marrow Transplantation.* Future Microbiol, 2014. **9**(10): p. 1117-21.
4. Maguire, G., *Therapeutics from Adult Stem Cells and the Hype Curve.* Acs Medicinal Chemistry Letters, 2016. **7**(5): p. 441-443.
5. Karanes, C., et al., *Twenty years of unrelated donor hematopoietic cell transplantation for adult recipients facilitated by the National Marrow Donor Program.* Biology of Blood and Marrow Transplantation, 2008. **14**(9): p. 8-15.
6. Herberts, C.A., M.S. Kwa, and H.P. Hermsen, *Risk factors in the development of stem cell therapy.* J Transl Med, 2011. **9**: p. 29.
7. Novotny, J. and F. Foret, *Fluid manipulation on the micro-scale: Basics of fluid behavior in microfluidics.* J Sep Sci, 2017. **40**(1): p. 383-394.
8. Yu, J., et al., *Microfluidics-based single-cell functional proteomics for fundamental and applied biomedical applications.* Annu Rev Anal Chem (Palo Alto Calif), 2014. **7**: p. 275-95.
9. McDonald, J.C., et al., *Fabrication of microfluidic systems in poly(dimethylsiloxane).* Electrophoresis, 2000. **21**(1): p. 27-40.
10. Bhatia, S.N. and D.E. Ingber, *Microfluidic organs-on-chips.* Nat Biotechnol, 2014. **32**(8): p. 760-72.
11. Jeong, H.H., D. Issadore, and D. Lee, *Recent developments in scale-up of microfluidic emulsion generation via parallelization.* Korean Journal of Chemical Engineering, 2016. **33**(6): p. 1757-1766.
12. Titmarsh, D.M., et al., *Concise Review: Microfluidic Technology Platforms: Poised to Accelerate Development and Translation of Stem Cell-Derived Therapies.* Stem Cells Translational Medicine, 2014. **3**(1): p. 81-90.
13. Xing, Y., et al., *A pumpless microfluidic device driven by surface tension for pancreatic islet analysis.* Biomedical Microdevices, 2016. **18**(5).
14. Ionescu-Tirgoviste, C., et al., *A 3D map of the islet routes throughout the healthy human pancreas.* Scientific Reports, 2015. **5**.
15. Thorens, B., *Neural regulation of pancreatic islet cell mass and function.* Diabetes Obesity & Metabolism, 2014. **16**: p. 87-95.
16. Kelly, C., N.H. McClenaghan, and P.R. Flatt, *Role of islet structure and cellular interactions in the control of insulin secretion.* Islets, 2011. **3**(2): p. 41-47.
17. DiGruccio, M.R., et al., *Comprehensive alpha, beta and delta cell transcriptomes reveal that ghrelin selectively activates delta cells and promotes somatostatin release from pancreatic islets.* Molecular Metabolism, 2016. **5**(7): p. 449-458.
18. Lonovics, J., et al., *Pancreatic-Polypeptide - a Review.* Archives of Surgery, 1981. **116**(10): p. 1256-1264.
19. Inui, A., et al., *Ghrelin, appetite, and gastric motility: the emerging role of the stomach as an endocrine organ.* Faseb Journal, 2004. **18**(3): p. 439-456.
20. Brissova, M., et al., *Assessment of human pancreatic islet architecture and*

composition by laser scanning confocal microscopy. Journal of Histochemistry & Cytochemistry, 2005. **53**(9): p. 1087-1097.
21. Hillage, H.L., *The Emerging Risk Factors Collaboration. Diabetes mellitus, fasting blood glucose concentration, and risk of vascular disease: a collaborative meta-analysis of 102 prospective studies (vol 375, pg 2215, 2010).* Lancet, 2010. **376**(9745): p. 958-958.
22. Zinman, B., et al., *American Diabetes Association. Standards of medical care in diabetes-2010 (vol 33, pg S11, 2010).* Diabetes Care, 2010. **33**(3): p. 692-692.
23. Robertson, R.P., *Medical progress: Islet transplantation as a treatment for diabetes - A work in progress.* New England Journal of Medicine, 2004. **350**(7): p. 694-705.
24. W., W.P., *Notes on diabetes treated with extract and by grafts of sheep's pancreas.* British Medical Journal, 1894(2): p. 2.
25. Ballinger, W.F. and P.E. Lacy, *Transplantation of Intact Pancreatic-Islets in Rats.* Surgery, 1972. **72**(2): p. 175-+.
26. Sutherland, D.E., et al., *Transplantation of dispersed pancreatic islet tissue in humans: autografts and allografts.* Diabetes, 1980. **29 Suppl 1**: p. 31-44.
27. Rossi, R.L., et al., *Segmental Pancreatic Autotransplantation with Pancreatic Ductal Occlusion after near Total or Total Pancreatic Resection for Chronic-Pancreatitis - Results at 5-Month to 54-Month Follow-up Evaluation.* Annals of Surgery, 1986. **203**(6): p. 626-636.
28. Wahoff, D.C., et al., *Autologous islet transplantation to prevent diabetes after pancreatic resection.* Ann Surg, 1995. **222**(4): p. 562-75; discussion 575-9.
29. Naftanel, M.A. and D.M. Harlan, *Pancreatic islet transplantation.* Plos Medicine, 2004. **1**(3): p. 198-201.
30. Scharp, D.W., et al., *Insulin Independence after Islet Transplantation into Type-I Diabetic Patient.* Diabetes, 1990. **39**(4): p. 515-518.
31. Shapiro, A.M.J., et al., *Islet transplantation in seven patients with type 1 diabetes mellitus using a glucocorticoid-free immunosuppressive regimen.* New England Journal of Medicine, 2000. **343**(4): p. 230-238.
32. Oberholzer, J., et al., *Human islet transplantation: lessons from 13 autologous and 13 allogeneic transplantations.* Transplantation, 2000. **69**(6): p. 1115-23.
33. Chhabra, P., D.E.R. Sutherland, and K.L. Brayman, *Overcoming barriers in clinical islet transplantation: Current limitations and future prospects.* Current Problems in Surgery, 2014. **51**(2): p. 49-86.
34. Lefebvre, P.J., et al., *Pulsatility of Insulin and Glucagon-Release - Physiological Significance and Pharmacological Implications.* Diabetologia, 1987. **30**(7): p. 443-452.
35. Arnold, M., *St. Paul and Protestantism : with an essay on Puritanism and the Church of England : and last essays on church and religion*. 1894, New York: Macmillan. xxxvii, 378 p.
36. Straub, S.G. and G.W.G. Sharp, *Glucose-stimulated signaling pathways in biphasic insulin secretion.* Diabetes-Metabolism Research and Reviews, 2002. **18**(6): p. 451-463.
37. Polonsky, K.S., B.D. Given, and E. Van Cauter, *Twenty-four-hour profiles and pulsatile patterns of insulin secretion in normal and obese subjects.* J Clin Invest, 1988. **81**(2): p. 442-8.

38. Ashcroft, F.M., D.E. Harrison, and S.J. Ashcroft, *Glucose induces closure of single potassium channels in isolated rat pancreatic beta-cells.* Nature, 1984. **312**(5993): p. 446-8.
39. Keizer, J. and G. Magnus, *Atp-Sensitive Potassium Channel and Bursting in the Pancreatic Beta-Cell - a Theoretical-Study.* Biophysical Journal, 1989. **56**(2): p. 229-242.
40. Gilon, P., et al., *Control mechanisms of the oscillations of insulin secretion in vitro and in vivo.* Diabetes, 2002. **51**: p. S144-S151.
41. Beauvois, M.C., et al., *Glucose-induced mixed [Ca2+](c) oscillations in mouse beta-cells are controlled by the membrane potential and the SERCA3 Ca2+-ATPase of the endoplasmic reticulum.* American Journal of Physiology-Cell Physiology, 2006. **290**(6): p. C1503-C1511.
42. Szollosi, A., et al., *Glucose stimulates Ca2+ influx and insulin secretion in 2-week-old beta-cells lacking ATP-sensitive K+ channels.* Journal of Biological Chemistry, 2007. **282**(3): p. 1747-1756.
43. Ashcroft, S.J., J.M. Bassett, and P.J. Randle, *Isolation of Human Pancreatic Islets Capable of Releasing Insulin and Metabolising Glucose in-Vitro.* Lancet, 1971. **1**(7705): p. 888-&.
44. Hopcroft, D.W., D.R. Mason, and R.S. Scott, *Standardization of Insulin-Secretion from Pancreatic-Islets - Validation of a DNA Assay.* Hormone and Metabolic Research, 1985. **17**(11): p. 559-561.
45. Norfleet, W.T., et al., *Comparison of alpha- and beta-cell secretory responses in islets isolated with collagenase and in the isolated perfused pancreas of rats.* Diabetes, 1975. **24**(11): p. 961-70.
46. Bentsi-Barnes, K., et al., *Detailed protocol for evaluation of dynamic perifusion of human islets to assess beta-cell function.* Islets, 2011. **3**(5): p. 284-90.
47. Dufrane, D., M. Nenquin, and J.C. Henquin, *Nutrient control of insulin secretion in perifused adult pig islets.* Diabetes & Metabolism, 2007. **33**(6): p. 430-438.
48. Haber, E.P., et al., *Palmitate modulates the early steps of insulin signalling pathway in pancreatic islets.* Febs Letters, 2003. **544**(1-3): p. 185-188.
49. Szkudelski, T., *The insulin-suppressive effect of resveratrol - An in vitro and in vivo phenomenon.* Life Sciences, 2008. **82**(7-8): p. 430-435.
50. Zawalich, W.S., et al., *Dexamethasone suppresses phospholipase C activation and insulin secretion from isolated rat islets.* Metabolism-Clinical and Experimental, 2006. **55**(1): p. 35-42.
51. Lacy, P.E., M.M. Walker, and C.J. Fink, *Perifusion of isolated rat islets in vitro. Participation of the microtubular system in the biphasic release of insulin.* Diabetes, 1972. **21**(10): p. 987-98.
52. Chen, D., et al., *The chemistrode: A droplet-based microfluidic device for stimulation and recording with high temporal, spatial, and chemical resolution.* Proceedings of the National Academy of Sciences of the United States of America, 2008. **105**(44): p. 16843-16848.
53. Dishinger, J.F. and R.T. Kennedy, *Serial immunoassays in parallel on a microfluidic chip for monitoring hormone secretion from living cells.* Analytical Chemistry, 2007. **79**(3): p. 947-954.
54. Rocheleau, J.V., et al., *Microfluidic glucose stimulation reveals limited coordination*

of intracellular Ca2+ activity oscillations in pancreatic islets. Proc Natl Acad Sci U S A, 2004. **101**(35): p. 12899-903.
55. Zhang, X.Y., et al., *Microfluidic System for Generation of Sinusoidal Glucose Waveforms for Entrainment of Islets of Langerhans.* Analytical Chemistry, 2010. **82**(15): p. 6704-6711.
56. Mohammed, J.S., et al., *Microfluidic device for multimodal characterization of pancreatic islets.* Lab Chip, 2009. **9**(1): p. 97-106.
57. Adewola, A.F., et al., *Microfluidic perifusion and imaging device for multi-parametric islet function assessment.* Biomedical Microdevices, 2010. **12**(3): p. 409-417.
58. Lee, D., et al., *Dual microfluidic perifusion networks for concurrent islet perifusion and optical imaging.* Biomedical Microdevices, 2012. **14**(1): p. 7-16.
59. Tan, W.H. and S. Takeuchi, *Dynamic microarray system with gentle retrieval mechanism for cell-encapsulating hydrogel beads.* Lab Chip, 2008. **8**(2): p. 259-266.
60. Nourmohammadzadeh, M., et al., *Microfluidic array with integrated oxygenation control for real-time live-cell imaging: effect of hypoxia on physiology of microencapsulated pancreatic islets.* Anal Chem, 2013. **85**(23): p. 11240-11249.
61. Walker, G. and D.J. Beebe, *A passive pumping method for microfluidic devices.* Lab Chip, 2002. **2**(3): p. 131-134.
62. J.Ju, J.Y.P., K.C Kim, H. Kim, E. Berthier, D.J. Beebe. S.H.Lee., *Backward flow in a surface tension driven miropump.* Journal of Micromechanics and Microengineering 2008. **18**: p. 087002.
63. Berthier, E. and D.J. Beebe, *Flow rate analysis of a surface tension driven passive micropump.* Lab Chip, 2007. **7**(11): p. 1475-1478.
64. Mata, A., A.J. Fleischman, and S. Roy, *Characterization of polydimethylsiloxane (PDMS) properties for biomedical micro/nanosystems.* Biomed Microdevices, 2005. **7**(4): p. 281-293.
65. Wang, Y., et al., *Systematic analysis of donor and isolation factor's impact on human islet yield and size distribution.* Cell Transplant, 2013. **22**(12): p. 2323-2333.
66. Santiago, J.G., et al., *A particle image velocimetry system for microfluidics.* Experiments in Fluids, 1998. **25**(4): p. 316-319.
67. Stull, N.D., et al., *Mouse Islet of Langerhans Isolation using a Combination of Purified Collagenase and Neutral Protease.* Jove-Journal of Visualized Experiments, 2012(67).
68. Adewola, A.F., et al., *Microfluidic perifusion and imaging device for multi-parametric islet function assessment.* Biomed Microdevices, 2010. **12**(3): p. 409-417.
69. Yamamoto, K., et al., *Fluid shear stress activates Ca(2+) influx into human endothelial cells via P2X4 purinoceptors.* Circ Res, 2000. **87**(5): p. 385-91.
70. Worley, J.F., 3rd, et al., *Endoplasmic reticulum calcium store regulates membrane potential in mouse islet beta-cells.* J Biol Chem, 1994. **269**(20): p. 14359-14362.
71. Zhang, X., et al., *Synchronization of mouse islets of Langerhans by glucose waveforms.* Am J Physiol Endocrinol Metab, 2011. **301**(4): p. E742-747.
72. Matthews, D.R., et al., *Pulsatile insulin has greater hypoglycemic effect than*

continuous delivery. Diabetes, 1983. **32**(7): p. 617-621.
73. Polonsky, K.S., et al., *Abnormal patterns of insulin secretion in non-insulin-dependent diabetes mellitus.* N Engl J Med, 1988. **318**(19): p. 1231-1239.
74. Shapiro, A.M., et al., *Islet transplantation in seven patients with type 1 diabetes mellitus using a glucocorticoid-free immunosuppressive regimen.* N Engl J Med, 2000. **343**(4): p. 230-238.
75. Ryan, E.A., et al., *Successful islet transplantation: continued insulin reserve provides long-term glycemic control.* Diabetes, 2002. **51**(7): p. 2148-2157.
76. Gangemi, A., et al., *Islet transplantation for brittle type 1 diabetes: the UIC protocol.* Am J Transplant, 2008. **8**(6): p. 1250-61.
77. Gray, H., W.H. Lewis, and Bartleby.com Inc., *Anatomy of the human body*. 2000, Bartleby.com: New York.
78. Frankenburg, W.K. and F.B. Rogers, *Hypoparathyroidism: review and case report.* Am Pract Dig Treat, 1959. **10**: p. 2130-4.
79. Ritter, C.S., et al., *Differential gene expression by oxyphil and chief cells of human parathyroid glands.* J Clin Endocrinol Metab, 2012. **97**(8): p. E1499-505.
80. Shoback, D., *Clinical practice. Hypoparathyroidism.* N Engl J Med, 2008. **359**(4): p. 391-403.
81. Kemper, B., *Molecular biology of parathyroid hormone.* CRC Crit Rev Biochem, 1986. **19**(4): p. 353-79.
82. Abate, E.G. and B.L. Clarke, *Review of Hypoparathyroidism.* Front Endocrinol (Lausanne), 2016. **7**: p. 172.
83. Clarke, B.L., et al., *Epidemiology and Diagnosis of Hypoparathyroidism.* Journal of Clinical Endocrinology & Metabolism, 2016. **101**(6): p. 2284-2299.
84. Rude, R.K., S.B. Oldham, and F.R. Singer, *Functional hypoparathyroidism and parathyroid hormone end-organ resistance in human magnesium deficiency.* Clin Endocrinol (Oxf), 1976. **5**(3): p. 209-24.
85. Bilezikian, J.P., et al., *Hypoparathyroidism in the adult: epidemiology, diagnosis, pathophysiology, target-organ involvement, treatment, and challenges for future research.* J Bone Miner Res, 2011. **26**(10): p. 2317-37.
86. Chan, J.C., et al., *Hypercalcemia in children with disorders of calcium and phosphate metabolism during long-term treatment with 1,25-dihydroxyvitamin-D3.* Pediatrics, 1983. **72**(2): p. 225-33.
87. Kurokawa, K., *Calcium-regulating hormones and the kidney.* Kidney Int, 1987. **32**(5): p. 760-71.
88. Christiansen, C., et al., *Deterioration of renal function during treatment of chronic renal failure with 1,25-dihydroxycholecalciferol.* Lancet, 1978. **2**(8092 Pt 1): p. 700-3.
89. Davies, M., *High-dose vitamin D therapy: indications, benefits and hazards.* Int J Vitam Nutr Res Suppl, 1989. **30**: p. 81-6.
90. Agha, A., et al., *Living-donor parathyroid allotransplantation for therapy-refractory postsurgical persistent hypoparathyroidism in a nontransplant recipient - three year results: a case report.* BMC Surg, 2016. **16**(1): p. 51.
91. Toledo, P.C., R.L. Rossi, and P. Caviedes, *Microencapsulation of Parathyroid Cells for the Treatment of Hypoparathyroidism.* Methods Mol Biol, 2017. **1479**: p. 357-363.

92. Murua, A., et al., *Cell microencapsulation technology: towards clinical application.* J Control Release, 2008. **132**(2): p. 76-83.
93. Weir, G.C., *Islet encapsulation: advances and obstacles.* Diabetologia, 2013. **56**(7): p. 1458-61.
94. Paredes Juarez, G.A., et al., *Immunological and technical considerations in application of alginate-based microencapsulation systems.* Front Bioeng Biotechnol, 2014. **2**: p. 26.
95. Sakai, S., et al., *Development of mammalian cell-enclosing subsieve-size agarose capsules (<100 microm) for cell therapy.* Biomaterials, 2005. **26**(23): p. 4786-92.
96. Cellesi, F., et al., *Towards a fully synthetic substitute of alginate: optimization of a thermal gelation/chemical cross-linking scheme ("tandem" gelation) for the production of beads and liquid-core capsules.* Biotechnol Bioeng, 2004. **88**(6): p. 740-9.
97. Sanchez, P., et al., *Encapsulation of cells in alginate gels.* Methods Mol Biol, 2013. **1051**: p. 313-25.
98. Smidsrod, O., *Molecular-Basis for Some Physical-Properties of Alginates in Gel State.* Faraday Discussions, 1975. **57**: p. 263-+.
99. Guisan, J.M., *Immobilization of Enzymes and Cells Third Edition Preface.* Immobilization of Enzymes and Cells, 3rd Edition, 2013. **1051**: p. V-V.
100. Morimoto, Y., et al., *Monodisperse semi-permeable microcapsules for continuous observation of cells.* Lab Chip, 2009. **9**(15): p. 2217-23.
101. Utech, S., et al., *Microfluidic Generation of Monodisperse, Structurally Homogeneous Alginate Microgels for Cell Encapsulation and 3D Cell Culture.* Adv Healthc Mater, 2015. **4**(11): p. 1628-33.
102. Agarwal, P., et al., *One-step microfluidic generation of pre-hatching embryo-like core-shell microcapsules for miniaturized 3D culture of pluripotent stem cells.* Lab Chip, 2013. **13**(23): p. 4525-33.
103. Madrigal, J.L., et al., *Microfluidic generation of alginate microgels for the controlled delivery of lentivectors.* Journal of Materials Chemistry B, 2016. **4**(43): p. 6989-6999.
104. Um, E.J., et al., *Multicompartment microfibers: fabrication and selective dissolution of composite droplet-in-fiber structures.* Journal of Materials Chemistry B, 2014. **2**(45): p. 7866-7871.
105. Liu, W.W., et al., *Fluorescence Identification of Parathyroid Glands by Aminolevulinic Acid Hydrochloride in Rats.* Photomedicine and Laser Surgery, 2011. **29**(9): p. 635-638.
106. Cury-Boaventura, M.F., et al., *Comparative toxicity of oleic and linoleic acid on human lymphocytes (vol 78, pg 1448, 2006).* Life Sciences, 2014. **112**(1-2): p. 97-97.
107. Martinez, C.J., et al., *A Microfluidic Approach to Encapsulate Living Cells in Uniform Alginate Hydrogel Microparticles.* Macromolecular Bioscience, 2012. **12**(7): p. 946-951.
108. Jung, S.Y., et al., *Standardization of A Physiologic Hypoparathyroidism Animal Model.* Plos One, 2016. **11**(10).
109. Duran, C.E., et al., *[Dynamics of calcium-regulated PTH secretion in secondary hyperparathyroidism: comparison between "in vivo" vs. "in vitro" responses].*

Nefrologia, 2010. **30**(1): p. 73-7.
110. Vegas, A.J., et al., *Long-term glycemic control using polymer-encapsulated human stem cell-derived beta cells in immune-competent mice (vol 22, pg 306, 2016).* Nature Medicine, 2016. **22**(4): p. 446-446.
111. Thomson, J.A., et al., *Embryonic stem cell lines derived from human blastocysts.* Science, 1998. **282**(5391): p. 1145-1147.
112. Takahashi, K., et al., *Induction of pluripotent stem cells from adult human fibroblasts by defined factors.* Cell, 2007. **131**(5): p. 861-872.
113. Pittenger, M.F., et al., *Multilineage potential of adult human mesenchymal stem cells.* Science, 1999. **284**(5411): p. 143-147.
114. Weissman, I.L., *Stem cells: Units of development, units of regeneration, and units in evolution.* Cell, 2000. **100**(1): p. 157-168.
115. Di Carlo, D. and L.P. Lee, *Dynamic single-cell analysis for quantitative biology.* Anal Chem, 2006. **78**(23): p. 7918-25.
116. Gumbiner, B.M., *Regulation of cadherin-mediated adhesion in morphogenesis.* Nature Reviews Molecular Cell Biology, 2005. **6**(8): p. 622-634.
117. Ahern, C.A. and R. Horn, *Stirring up controversy with a voltage sensor paddle.* Trends in Neurosciences, 2004. **27**(6): p. 303-307.
118. Geiger, B. and A. Bershadsky, *Exploring the neighborhood: Adhesion-coupled cell mechanosensors.* Cell, 2002. **110**(2): p. 139-142.
119. Helmke, B.P. and P.F. Davies, *The cytoskeleton under external fluid mechanical forces: Hemodynamic forces acting on the endothelium.* Annals of Biomedical Engineering, 2002. **30**(3): p. 284-296.
120. Lucchetta, E.M., et al., *Dynamics of Drosophila embryonic patterning network perturbed in space and time using microfluidics.* Nature, 2005. **434**(7037): p. 1134-1138.
121. Mycielska, M.E. and M.B.A. Djamgoz, *Cellular mechanisms of direct-current electric field effects: galvanotaxis and metastatic disease.* Journal of Cell Science, 2004. **117**(9): p. 1631-1639.
122. Rustom, A., et al., *Nanotubular highways for intercellular organelle transport.* Science, 2004. **303**(5660): p. 1007-1010.
123. Wei, C.J., X. Xu, and C.W. Lo, *Connexins and cell signaling in development and disease.* Annual Review of Cell and Developmental Biology, 2004. **20**: p. 811-838.
124. Meier, S.M., H. Huebner, and R. Buchholz, *Single-cell-bioreactors as end of miniaturization approaches in biotechnology: progresses with characterised bioreactors and a glance into the future.* Bioprocess and Biosystems Engineering, 2005. **28**(2): p. 95-107.
125. Nilsson, J., et al., *Review of cell and particle trapping in microfluidic systems.* Analytica Chimica Acta, 2009. **649**(2): p. 141-157.
126. Wheeler, A.R., et al., *Microfluidic device for single-cell analysis.* Analytical Chemistry, 2003. **75**(14): p. 3581-3586.
127. Keenan, T.M. and A. Folch, *Biomolecular gradients in cell culture systems.* Lab on a Chip, 2008. **8**(1): p. 34-57.
128. Di Carlo, D., N. Aghdam, and L.P. Lee, *Single-cell enzyme concentrations, kinetics, and inhibition analysis using high-density hydrodynamic cell isolation arrays.* Analytical Chemistry, 2006. **78**(14): p. 4925-4930.

129. Kimmerling, R.J., et al., *A microfluidic platform enabling single-cell RNA-seq of multigenerational lineages.* Nature Communications, 2016. **7**.
130. Kobel, S.A., et al., *Automated analysis of single stem cells in microfluidic traps.* Lab on a Chip, 2012. **12**(16): p. 2843-2849.

VITA

EDUCATION

Ph. D. in Biomedical and Biological Engineering
University of Illinois at Chicago, Chicago, IL Jan. 2014 - Present

M. S. in Cell and Molecular Biology
Illinois Institute of Technology, Chicago, IL Jan. 2011 - Dec. 2012

B. S. in Biology
Wuhan University, Wuhan, Hubei, P. R. China Sep. 2006 - Jun. 2010

RESEARCH EXPERIENCE

Research Intern June. 2017 - Present
University of Virginia, Charlottesville, VA
- Designed novel microfluidic platforms for single cell imaging and analysis
- Designed organ-on-chip model for studies of cell-cell or cell-bacteria interaction
- Performed microfluidic perfusion-based tests for stem cell studies
- Fabricated the micro-encapsulated parathyroid cells on-chip for transplantation

Graduate Research Assistant May. 2013 - May. 2017
University of Illinois at Chicago, Chicago, IL
- Designed a novel surface tension driven pumpless microfluidic platforms for pancreatic islet physiological research
- Designed a flow-focusing-based micro-encapsulator device for single cell encapsulation
- Designed a dual-chamber perfusion system for cell imaging and analysis at single cell level
- Performed many *in vitro* / *in vivo* tests for new drug development and stem cell studies
- Performed small rodent animal surgery of islet isolation and transplantation
- Conducted histological studies of pancreas and liver samples

Teaching Assistant Jan. 2014 - May. 2016
University of Illinois at Chicago, Chicago, IL
- Assisted the instructors in teaching, grading and team leading in several courses either at undergraduate or graduate level

Research Project Member Jan. 2012 - Dec. 2012
Illinois Institute of Technology, Chicago, IL
- Designed a dystrophin-targeted vector with specific self-assembly components containing overlapping regions
- Assembled the plasmid and transformed into bacteria cell culture for screening by selectable marker
- Developed the knockout mice for a closer study to dystrophin

Undergraduate Research Assistant Oct. 2007 - Jun. 2010
State Key Laboratory of Virology, Wuhan, Hubei, P. R. China
- Isolated and cultured different types of primary cells to set up multiple viruses' infection models
- Detected the virus infection with immunochemistry probes and extracted viral epitope genes

with cloning technique
- Evaluated the interactions between proteins and the potential relations between enzymatic activity of methylase, cytokines production and virus infection
- Completed B.S. degree thesis "A screen for epigenetic modification-related proteins interacted with NS1, an important influenza virus non-structure protein" in Jun. 2010

Research Intern Sep. 2009 - Jan. 2010
Key Laboratory of Plant Developmental Biology (Wuhan University), Ministry of Education, P. R. China
- Induced mutation on seeds of Arabidopsis by estrogen contained culture
- Extracted mRNA and built cDNA library for genetic analysis
- Performed the cross-seeding of mutants to select the desirable traits

Field Survey Intern July. 2008
Research Station of Shennongjia Nature Reserve, Hubei, P. R. China
- Participated in the field observations and studies in Shennongjia Natural Reservation Area

ACTIVITIES

Olympic Volunteer July. 2008 - Aug. 2008
The 29th Olympic Games, Beijing, P. R. China
- Coordinated ticket checking, distribution of match information and provided language or guide service to visitors

Host of the University Freshman Orientation Sep. 2006 - Feb. 2007
School of Resource and Environmental Sciences, Wuhan University, Wuhan, Hubei, P. R. China
- Hosted, organized and participated in large-scaled activities like "University Freshman Welcome Party" and "Department Annual Award Ceremony" in 2006-2007 academic year in the school of Resource and Environmental Sciences

Department Newspaper Editor and Reporter Sep. 2006 - Feb. 2007
School of Resource and Environmental Sciences, Wuhan University, Wuhan, Hubei, P. R. China
- Wrote and edited news and for school official newspaper and website and took photographs as a reporter in the field

SKILLS

Lab:
1. Molecular Biology: cloning, PCR (RT-PCR, real time PCR, cloning PCR, etc.), DNA and RNA extraction, lymphocyte isolation, cell culture, virus culture, transformation, transfection, ELISA, western blot, yeast two-hybrid system, luciferase assay, etc.
2. Biomedical Engineering: design and fabrication of microfluidic devices, micro-encapsulation, pancreatic islet isolation, *in vitro* cell perfusion for drug screening, fluorescent and confocal microscopy, tissue histology, etc.

Software Proficiencies: AutoCAD, COMSOL Multiphysics, SolidWorks, 3DS MAX, Blender, Matlab, Windows/Mac OS system, Microsoft Office Software, Clone manager, Primer Premier, Serial Cloner, Cn3D, Swiss-Pdbviewer, etc.

Language: Chinese (Mandarin) and English

PUBLICATIONS

1. **Xing Y**, Nourmohammadzadeh M, Elias JE, Chan M, Chen Z, McGarrigle JJ, Oberholzer J, and Wang Y. A pumpless microfluidic device driven by surface tension for pancreatic islet analysis. *Biomed Microdevices*. 18:80. (2016)

2. **Xing Y**, Xie K, Chan M, Poon H, Wang M, Wang S, Qi M, and Wang Y. Development of microfluidic devices for islet transplantation and islet physiology. *Prac J Organ Transplant*. 4:334-40. (2016)

3. Nourmohammadzadeh M, **Xing Y**, Lee JW, Bochenek MA, Mendoza-Elias JE, McGarrigle JJ, Marchese E, Yeh CC, Eddington DT, Oberholzer J, and Wang Y. A microfluidic array for real-time live-cell imaging of human and rodent pancreatic islets. *Lab Chip*. 16:1466-72. (2016)

4. Chakravarthy H, Gu XY, Enge M, Dai XQ, Wang Y, Damond N, Downie C, Liu K, Wang J, **Xing Y**, Chera S, Thorel F, Quake S, Oberholzer J, MacDonald PE, Herrera PL, and Kim SK. Converting adult pancreatic α-cells into β-cells by targeting Dnmt1 and Arx. *Cell Metab.* 25:622-634. (2017)

5. McGarrigle JJ, Omami M, Reedy M, Isa D, Ghani S, Marchese E, Bochenek MA, Long M, **Xing Y**, Joshi I, Wang Y, and Oberholzer J. Islet Microencapsulation: Strategies and Clinical Status in Diabetes. *Curr Diab Rep*. 17:47. (2017)

6. Sui L, Danzl N, Campbell SR, Viola R, Williams D, **Xing Y**, Wang Y, Phillips N, Johannesson B, Oberholzer J, Powers AC, Leibel RL, Chen XJ, Sykes M, and Egli D. Beta cell replacement in mice using human type 1 diabetes nuclear transfer embryonic stem cells. *Diabetes*. (accepted and epub in Sep. 2017)

7. Ji YW, Sun SY, Shrestha N, Darragh L, **Xing Y**, He Y, Carboneau BA, Kim GH, Kim H, Xin S, Oberholzer J, Soleimanpour S, Gannon M, Liu CY, Naji A, Kulkarni R, Wang Y, Kersten S, and Qi L. Toll-like receptors 2 and 4 control adaptive beta-cell expansion in diet-induced obesity. *Nat Immunol.* (submitted in May. 2017)

8. Nair GG, Liu J, Russ HA, Tran S, Saxton M, Chen R, **Xing Y**, Wang Y, Nguyen VQ, Szot G, Oberhozler J, Bhushan A, and Hebrok M. Recapitulating endocrine cell clustering promotes formation of mature beta cells from human stem cells. *Nat Biotechnol.* (submitted in Mar. 2017)

9. Chan MW*, **Xing Y***, Nourmohammadzadeh M, Mendoza-Elias JE, Poon H, He Y, Yeh J, McGarrigle JJ, Oberholzer J, and Wang Y. Smartphone-Fluidics Based Flow Cytometry for Human Islet Mass Quantification. *Lab Chip.* *Equal contribution (under peer review)

10. Wang Y, Danielson KK, McGarrigle JJ, Gutierrez D, Ropski A, Marchese E, Barbaro B, Nourmohammadzadeh M, Qi M, Mendoza-Elias JE, **Xing Y**, Monson RS, Eddington DT, and Oberholzer J. Intracellular calcium and GSIS can be used together to predict *in vivo* islet function. *American Journal of transplant.* (under peer review)

11. Wang Y, Qi M, McGarrigle JJ, **Xing Y**, Zeng LY, Mendoza-Elias JE, Bochenek M, Marchese E, He Y, Oberholzer J. Diazoxide preconditioning of non-human primate pancreas in procurement and preservation improves islet isolation outcomes and function. *American Journal of transplant.* (under peer review)